To the Graduate Council:

I am submitting herewith a thesis written by Sangeetha Swaminathan entitled "Fabrication of Nano-Injection Needles for Neural Pathway Study in Mice." I have examined the final electronic copy of this thesis for form and content and recommend that it be accepted in partial fulfillment of the requirements for the degree of Master of Science, with a major in Electrical Engineering.

Jie Wu, Major Advisor

We have read this thesis
and recommend its acceptance:

Hairong Qi

Mohamed Mahfouz

Accepted for the Council:
Carolyn R. Hodges

Vice Provost and Dean of the
Graduate School

(Original signatures are on file with official student records.)

# Fabrication of Nano-Injection Needles for Neural Pathway Study in Mice

A Thesis

Presented for the

Master of Science Degree

The University of Tennessee, Knoxville

**Sangeetha Swaminathan**

August 2007

*This thesis is dedicated to my parents,*
*Dr. Thangam Swaminathan and Dr. S. V. Swaminathan,*
*my sister, Sandy Sree and my brother-in-law, Sai Hari*
*for always inspiring me and being there for me, period.*

# ACKNOWLEDGEMENTS

Firstly, I would like to thank God for giving me the ability to pursue my goals and for surrounding me with kind and supportive people.

My overwhelming thanks go to my graduate and thesis advisor, Dr. Jie Wu, for her invaluable guidance, support, motivation and patience throughout the entire course of my study. A very accommodating and considerate person, she is actively involved in the work of all her students, and always has their best interests in mind. I could not have imagined a better advisor, without whose knowledge and perceptiveness I would not have finished this thesis. I am grateful to her for giving me an opportunity to work on this topic.

I would like to thank Dr. Gary Bernstein, for allowing me the use of the excellent facilities of the Notre Dame Nanofabrication Facility (NDNF, University of Notre Dame, Indiana) and providing valuable guidance. Specifically, I would like to thank Keith Darr, Mark Richmond and Michael Thomas who taught me how to work with the various equipments and patiently dealt with all my questions. Dr. Botond Roska, the collaborator of this project, for his inestimable feedback. Yesenia Bernal and John Baeten, who were elemental in the completion of this thesis, and VJ for all the help with the SEM.

I also wish to thank my committee members, Dr. Hairong Qi and Dr. Mohamed Mahfouz, for obliging to serve as my thesis committee and for their intellectual support.

A special thanks to the staff and students at the Innovative Technology Center (ITC – where I could stay late at nights and weekends), who are more like a family to me, always happy to hear my outrage or glee at the progress of my thesis, encouraging me all the time with warm smiles, wondering if I ever went home!

Thanks to my close friends who always stood by my side asking over and over again, “When will you get it done? Next week? Next month? When?”; Bala, for forever digging out papers, articles and free online books that he thought might even remotely help me with my work, and for all the proof-reading; Chandra, for being the best room-mate ever.

Lastly, and most importantly, I wish to thank my parents, Dr. Thangam Swaminathan and Dr. S. V. Swaminathan, sister, Sandya Sree and brother-in-law, Sai Hari for their unconditional love and absolute confidence in me.

# ABSTRACT

The potential of micro-needles to provide an interconnection between the microscopic and the macroscopic worlds makes it one of the most revolutionary fields in health care, allowing for precise transdermal drug delivery of highly targeted small doses of the active compound. Current micro electro mechanical systems (MEMS) technologies, originally designed for the micro-electronics industry, have been utilized in the fabrication of different micro-needle designs and their integration with various micro-fabricated micro-fluidics devices. The target of this thesis is to achieve a micro-needle injection system to deliver several strains of pico-liter volumes of a fluid combination of transgenic virus and luminescent compound, to be injected into the visual cortex of mice in order to study the structure and function of the neural networks of the brain. Micro-needles having a body dimension of 10 mm x 10 mm and a shaft 1 mm wide and 3 mm long have been constructed from silicon wafers, using technologies originally developed for integrated circuit (IC) fabrication. Silicon wafers have also been used in the fabrication of the needle channels having a width of 4 μm and a total depth of 60 μm with a 20 μm deep channel at the base of the 40 μm trench. Both wet and dry bulk micromachining techniques have been used to create the needle bodies and channels. The optimum fabrication method has been found to be the deep reactive ion etching (DRIE) and $SiO_2$ deposition using the plasma enhanced chemical vapor deposition (PECVD) has been used to seal the channels.

# TABLE OF CONTENTS

**Chapter 1 Introduction** ..... 1
1.1 Introduction ..... 1
1.1.1 Motivation ..... 2
1.1.2 Background ..... 4
**Chapter 2 Literature Review and Research Plan** ..... 9
2.1 Literature Review ..... 9
2.1.1 Out of Plane Microneedles ..... 10
2.1.2 In-Plane Microneedles ..... 12
2.1.3 In-Plane Microneedles with Buried Channels ..... 16
2.2 Research Plan ..... 22
2.2.1 Micro-needle Design ..... 22
2.2.2 Mask Material ..... 24
2.2.3 Fabrication Process ..... 25
**Chapter 3 Photomask Generation and Lithography** ..... 27
3.1 Photomask ..... 27
3.2 Photolithography ..... 28
3.2.1 Photoresist ..... 29
3.2.2 Image Reversal ..... 30
3.2.3 Lift – off ..... 32
3.2.4 Alignment Marks ..... 33
**Chapter 4 Buried Channel Fabrication** ..... 35
4.1 KOH Etching ..... 35
4.1.1 Silicon Structure ..... 35
4.1.2 Anisotropic Wet Chemical Etching ..... 36
4.2 DRIE ..... 39
4.2.1 Plasma Generation ..... 39
4.2.2 Standard Bosch Process ..... 39
4.2.3 Using Bosch Process to Etch Microchannels ..... 40

4.2.4 Modified Bosch Process ..... 43
4.3 Channel Sealing – PECVD ..... 47
4.3.1 PECVD Oxide ..... 47
**Chapter 5 Microneedle Body Fabrication** ..... 49
5.1 KOH Etching ..... 49
5.1.1 Chromium/Gold (Cr/Au) ..... 50
5.1.2 PECVD Silicon Nitride ..... 53
5.1.3 LPCVD Silicon Nitride ..... 56
5.2 DRIE ..... 58
5.2.1 Photoresist Mask ..... 58
5.2.2 Aluminum Mask ..... 59
**Chapter 6 Results and Discussion** ..... 61
6.1 Microchannel ..... 61
6.2 Channel Sealing ..... 61
6.3 Needle Body ..... 63
**Chapter 7 Conclusions and Future Work** ..... 66
**References** ..... 69
**Vita** ..... 74

# LIST OF TABLES

Table 1.1: Summary of microchannel cross-sections and fabrication techniques ..... 5
Table 2.1: Process schemes for BCT ..... 17
Table 2.2: Design variation in micro-needle shaft ..... 20
Table 4.1: Summary of process steps used in anisotropic wet etching ..... 36
Table 4.2: Standard parameters for the Bosch process in Alcatel 601E ICP..... 41
Table 4.3: Process steps and parameters for the revised Bosch process..... 44

# LIST OF FIGURES


Figure 1.1: [Left] Top view of a mouse's skull where the needle needs to be injected; [Right] Image of nearby ganglion cells in visual cortex of mouse ..... 4

Figure 1.2: [Left] Isotropic etch profile; [Right] Anisotropic etch profile ..... 7

Figure 2.1: Out of plane silicon micro-needles ..... 10

Figure 2.2: [Left]Fabrication process schematics for Gardeniers et al; [Right] Out of plane hollow microneedle ..... 11

Figure 2.3: Steps involved in the fabrication process for Lin et al ..... 13

Figure 2.4: [Left] Top view of the needle and its reservoir; [Right] View of the cross-section of the micro-channel ..... 13

Figure 2.5: Process flow for fabrication of bulk titanium micro-needles ..... 15

Figure 2.6: SEM image of [Left] embedded microfluidic networks before bonding; [Right] fluid ports on the side ..... 15

Figure 2.7: [Left] Different shapes of micro channels; [Right] Circular channel etched electrochemically in 5% HF solution .... 16

Figure 2.8: Fabrication steps involved in the process created by Chen et al ..... 19

Figure 2.9: [Left] Closely fitted chevron structures over the channel; [Right] View of a cross-section of the etched microchannel ..... 19

Figure 2.10: Schematic of microneedle, process flow for cross-sections A-A′, B-B′ .. 21

Figure 2.11: SEM images [Top] fabricated micro-needle; [A] micro-channel entrance at reservoir; [B] micro-channel entrance at tip of micro-needle ..... 21

Figure 2.12: [Left] Graphic of micro-needle insertion into visual cortex of a mouse [Right] Schematic of needle proposed..... 22

Figure 2.13: Schematic of the micro-channel in the needle proposed..... 24

Figure 2.14: Process flow for the fabrication of the micro-channels..... 26

Figure 2.15: Process flow for the fabrication of the micro-needle body ..... 26

Figure 2.16: Example of integrated microneedle microfluid chip ..... 26
Figure 3.1: Screen view of a proposed microneedle pattern designed on L-Edit ..... 28
Figure 3.2: Schematic of photolithographic process ..... 30
Figure 3.3: Schematic of results obtained by positive and negative photoresists..... 31
Figure 3.4: Process sequence for image reversal in a positive photoresist..... 31
Figure 3.5: Lift-off sequence with positive photoresist..... 33
Figure 3.6: Double sided alignment schematic..... 34
Figure 4.1: Arrangement of atoms (a) silicon crystal lattice; (b) (100), (111) planes . 35
Figure 4.2: Schematic of: (a) (100) plane; (b) (111) plane; (c) anisotropic etching of silicon in (100) plane tending to expose the (111) plane ..... 38
Figure 4.3: Schematic of anisotropic etching of rectangular opening ..... 38
Figure 4.4: Anisotropic characteristic of wet chemical etching ..... 38
Figure 4.5: Flow rate plot of gases during etch and passivation processes over time . 40
Figure 4.6: [Left] Scalloped sidewalls
[Right] SEM image of high density tip etched in Bosch process ..... 41
Figure 4.7: Alpha Step 500 Profiler graphs of width of microchannel opening..... 42
Figure 4.8: SEM image of the needle reservoir with microchannel inlet ..... 45
Figure 4.9: Alpha Step 500 Profiler graphs of width of microchannel opening……46
Figure 4.10: SEM image of an anisotropically etched channel sealed with $SiO_2$..... 48
Figure 4.11: SEM image of top view of the sealed microchannel..... 48
Figure 5.1: Microscope image of a patterned 50Å/2000Å Cr/Au coated wafer..... 50
Figure 5.2: Picture of a needle released after 5.5 hours of KOH etching ..... 51
Figure 5.3: Picture of the brittle needle bodies..... 52
Figure 5.4: Microscope image of needle after 3 hours of KOH etching..... 52
Figure 5.5: Print screen image of the new needle body design created on L-Edit ..... 52
Figure 5.6: Microscope image of needle after 2 hours of KOH etching..... 53
Figure 5.7: Microscope image of the needle body after 3 hours of KOH etching..... 54
Figure 5.8: Microscope image of pattern on 6000Å of PECVD silicon nitride ..... 55
Figure 5.9: Microscope image of needles after 2 hours of KOH etching..... 55
Figure 5.10: Microscope image needles after 2 hours of KOH etching ..... 55

Figure 5.11: Microscope image of released needle after 4.5 hours of KOH etching ..... 57
Figure 5.12: Microscope image of released needle after 4.5 hours of KOH etching ..... 57
Figure 5.13: Print screen image of the needle design created on L-Edit ..... 58
Figure 5.14: Picture of completely etched needle bodies with aluminum mask intact... 60
Figure 5.15: Microscope image of the released needle with aluminum mask..... 60
Figure 5.16: SEM image of back-side of released needle with aluminum mask on top..60
Figure 6.1: SEM image of microchannel at 300 X magnification..... 62
Figure 6.2: Schematic of the desired circular microchannel ..... 62
Figure 6.3: SEM image of the microchannel formed during the isotropic etch cycle .. 62
Figure 6.4: SEM image of a channel sealed partially with PECVD silicon dioxide .... 64
Figure 6.5: SEM image of back side of needle released using revised Bosch process. 64
Figure 6.6: SEM image of unpolished side of needle..... 65
Figure 6.7: Close-up SEM image of the unpolished side of needle released ..... 65
Figure 6.8: Microscope image of microneedle body ..... 65
Figure 7.1: Example of microneedle interfaced with a mechanical pump ..... 66
Figure 7.2: Schematic of the base to house the microneedle..... 67
Figure 7.3: CADKEY design of the top part of the mechanical interface unit..... 67
Figure 7.4: Schematic of extended handle integrated with mechanical pump unit ..... 67
Figure 7.5: Schematic of a microneedle containing multiple outlet ports ..... 68

# CHAPTER 1 INTRODUCTION

## 1.1 Introduction

Advances in biotechnology and the processing of materials on a micro-scale level have motivated researchers in these fields to develop novel applications in the field of bio-medicine today. One significant application area is micro-needle arrays fabricated based on the micro electro mechanical systems (MEMS) technology. Micro-needles are prepared either singularly or in arrays, usually incorporating techniques that involve one or more technologies that enable the precise machining, extrusion, casting and/or forming of such needles. There has been much research aimed at creating micro-needles in large batches from inexpensive metal and polymer materials [1].

Minimally invasive drug delivery devices use tiny needles – micro-needles – to transfer drugs effectively by penetrating the outer layer of the skin, thereby allowing transdermal absorption of the active compound. These needles are, for most part, of (or smaller than) the diameter of a strand of human hair and can deliver the desired drug in a nearly painless and highly localized manner, by penetrating just under or just below the stratum corneum (the top layer of the skin that has very low permeability), hence avoiding puncturing nerves and reducing the chances of pain, infection or injury. Micro-needle arrays fabricated based on the micro electro-mechanical system (MEMS) technology find significant applications in the field of biomedicine today. Reference [2], for example, describes a disposable subcutaneous glucose monitor consisting of hollow micro-needles. Also, since blood sampling for testing and multiple doses of insulin for sugar require the frequent use of needles, the use of a micro-needle or micro-needle patches can make it a virtually pain-free experience. Biodegradable micro-needles are also available which can be disintegrated and dispersed into the human skin [3]. Apart from painless injection devices, micro-needles can also be used in many other fields such as genetic engineering for introducing DNA into cells [4], and micro-dialysis where the micro-needles

developed are permeable to small molecular weight compounds, so that the sensors connected to the medical monitors may be protected from higher molecular weight compounds like proteins [5].

This thesis is targeted at achieving a micro-needle injection system that would deliver pico-liter volumes of transgenic virus combined with a luminescent chemical, into the visual cortex of mice. In order to accomplish this, needles are fabricated using silicon wafers, via micro-machining technology used for batch fabrication. Silicon is an active material with excellent mechanical properties [6] that is abundant and hence, inexpensive. Other factors that make silicon a good choice for making the needles are that, apart from being well suited for miniaturization, it can be processed to high levels of purity. Also, since many needles can be fabricated on a single substrate due to the small size, this implies more accuracy and more reproducibility. With silicon wafers, in-plane as well as out of plane needles can be created, thereby providing higher flexibility with respect to different needles designs.

### *1.1.1 Motivation*

MEMS technology has played a vital role in many key areas such as medicine, transportation, defense systems, communication, environmental-monitoring, automated manufacturing, bio-technology, and consumer products. As mentioned before, factors like reduced size, low manufacturing cost, light weight, lesser power and heat dissipation, and improved speed have made MEMS devices most sought after today. The growth of MEMS in the field of micro-fluidics, and the drive to fabricate devices of the same size as the biological entity of interest has led into the development of wide variety of micron size devices such as micro-total-analysis system (μ-TAS) [7] and silicon bio-capsules [8] has led to the expansion of MEMS in the field of micro-biotechnology too. Micro-biotechnology has roots both in the semiconductor industry as well as life sciences. It forms the basis of most of the basic research in the field of biology. The integration of

small scale with functionality, in order to solve for bio-analytical problems, has spurred an interest in finding new and effective solutions to problems in the realms of biology, biomedicine and genome sciences.

Today, most research in this field is focused at simplifying drug delivery systems. Drug delivery is primarily of two kinds; orally administered pills and hypodermic needles. Injection systems that can administer highly targeted small doses of the active fluid compound are desired, so that the poor absorption and deterioration of the liver and intestines from pills, as well as the pain caused by conventional injections may be avoided. An example of one of the smallest needles commercially available today, 30 gauge needles have a wall thickness of 76 μm and an outer diameter of 305 μm [9]. Micro-needles are highly sharp devices having tips of sizes in the sub-micron range. The application desired for this thesis is a micro-needle injection system that will deliver pico-liter volumes of a transgenic viral fluid, combined with a luminescent compound, into the visual cortex of mice.

The purpose of the experiment with the mice is to study the structure and function of the neural networks of the brain. The idea is to inject the optical cortex of mice with viruses, whose DNA have been modified to fluorescence, to observe the networking of the nearby ganglion cells. Then the activity of each neuron is recorded with the aid of retinal light simulation, as the virus replicates itself along the optical paths to reveal the neural interconnections between the cortex and the eye, as shown in Figure 1.1. Several strains of the virulent fluid need to be injected simultaneously in order to observe the neural pathways efficiently. Also, an important factor that needs to be kept in mind is that the size of the visual cortex of mice is only about one or two millimeters across. The fabrication of needles with sharp edges that would produce the least amount of damage to the visual cortex and deliver the precise volume of fluid at the point of insertion is required. This can be successfully achieved only via MEMS technology.

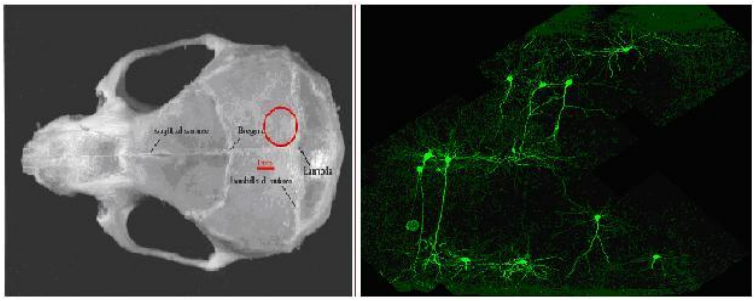

Figure 1.1: [Left] Top view of a mouse's skull where the needle needs to be injected; [Right] Low resolution image of nearby ganglion cells in the visual cortex of mouse's brain after being injected with a transgenic virus tagged with luminescent compound [Figures obtained from Dr. Botond Roska]

### *1.1.2 Background*

Microfabrication is a collective term for the manufacturing technologies used in the making of components on a micrometer sized scale, such as integrated circuits or MEMS. Micro-Electro-Mechanical Systems (MEMS) are devices that generally range in size from micrometers to a few millimeters and have electrical as well as mechanical functionality. These devices are batch fabricated using micro-fabrication techniques that were initially developed for the semiconductor industry. Examples of such technologies that aid fabrication of very small devices include molding and plating, wet and dry etching, and electro discharge machining (EDM). MEMS has received much attention due to increased miniaturization and higher performance, compared to conventional devices. Due to the small size and due to the use of already available IC manufacturing processes, the cost of fabricating these devices is lower than most macro devices. In IC fabrication, hundreds of units are produced simultaneously on a single wafer (batch processing). Hence, large volumes of the device can be produced at a low cost. Also, the electrical and thermal response times of these devices are smaller, owing to their small size.

Microfluidics is a multi-disciplinary field comprising physics, chemistry, engineering and biotechnology and deals with the behavior, control and manipulation of fluids at the micro-scale. The devices used in this field are those that have one or more channels with at least one dimension less than 1 mm. Most microfluidic devices are used in biomedical research. This is because the volume of fluids used in these channels is usually in the order of nanoliters and the fabrication techniques used to construct these devices are relatively inexpensive, even for mass production. Examples of microfluidic devices include microvalves, micropumps, microchannels, sensors etc. These devices are fabricated using various technologies such as bulk micromachining, Deep Reactive Ion Etching (DRIE), surface micromachining, LIGA, etc. Table 1.1 shows different fabrication techniques used to create microchannels [12].

According to Madou [10], bulk micromachining is that part of micro-fabrication where three dimensional features are etched into the bulk of the crystalline or non-crystalline material. In bulk micromachining, the desired pattern is transferred onto a substrate from the mask via photolithography, and then, starting at the substrate, the required pattern is etched into the substrate. Bulk micromachining can be performed on dry as well as wet etching processes.

**Table 1.1: Summary of microchannel cross-sections and appropriate fabrication techniques [12]**

| Channel Shapes | BM | SM | H | CM | WB |
|---|---|---|---|---|---|
| | ✔ | | ✔ | ✔ | |
| 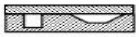 | ✔ | | ✔ | ✔ | ✔ |
| | ✔ | | | ✔ | |
| 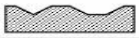 | ✔ | | | | |
| | ✔ | | | | |
| | ✔ | ✔ | | | |
| 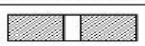 | ✔ | | ✔ | ✔ | |
| 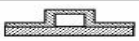 | | ✔ | | | |

BM = bulk micromachining
SM = surface micromachining
H = high aspect ratio machining
CM = conventional machining
WB = wafer bonding

Removal of material from a substrate by exposing it to the bombardment of ions at the surface of the substrate, thereby forcing out portions of the substrate is called dry etching. The reactants required for this type of etching are in the gas or vapor phase and usually ionized. The different dry etch mechanisms include gas phase etch and RF plasma based etch. In the gas phase etch, the reactive gas molecules adsorb on the surface of the substrate, react with the substrate and dissociate the material. RF plasma etch is achieved when an electric field is applied to the gas, causing it to break down into fully or partially ionized gas having equal number of positive and negative charges and a different number of unionized molecules. These dry etch mechanisms are used to classify the dry etch methods into physical and chemical etch. During the physical etch, mechanical or physical interaction between the gas molecules and the substrate's surface takes place when positively charged ions bombard the surface with high kinetic energy, thereby leading to material removal from the substrate. An example of physical etch is the sputtering etch. In the chemical etching method, neutral and/or ionized molecules interact with the material surface to produce volatile products. It is also possible to use physical and chemical dry etch methods in combination.

Wet etching involves the use of chemical etchers to dissolve away unwanted materials. Here, when the wafer is immersed in a liquid bath of chemical etchers, there occurs a transport of the reactants to the surface of the wafer, reaction of these chemicals at the surface of the substrate, and a transport of the products of reaction from the surface of the substrate. The three key ingredients in the wet etching process are: an oxidizer (e.g. hydrogen peroxide), an acid or a base to dissolve the oxidized surface (e.g. ammonium hydroxide), and a diluting agent for transport (e.g. water). The chemical etchers used in the wet etching process are of two types; isotropic etcher and anisotropic etcher.

Isotropic etchers are independent of the orientation of the mask edge and have a lateral etch rate almost the same as the vertical etch rate. The resulting geometries are not bound by predefined crystallographic planes (Figure 1.2- Left). However, the etch rate is temperature as well as agitation sensitive. Wet isotropic etchers are usually acidic like

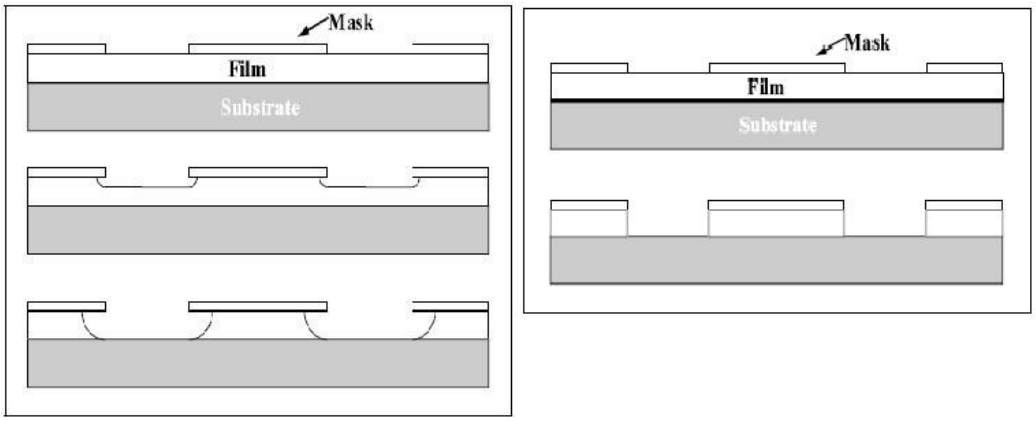


Figure 1.2: [Left] Isotropic etch profile; [Right] Anisotropic etch profile [11]

Piranha (4:1 $H_2O_2$: $H_2SO_4$), buffered HF (5:1 $NH_4F$: HF) and HNA ($HF/HNO_3/CHCOOH$), and typically chemically ionized gas (plasma) or fluorine containing gases (non-plasma) for dry isotropic etching.

Anisotropic etchants, on the other hand, require substrates having a well defined crystalline structure. This type of etching is preferred where straight walls are essential (Figure 1.2- Right). Depending on the orientation of the mask edge, with respect to the crystalline axes, the lateral etch rates can be greater or lesser than the vertical etch rates. Anisotropic etching is much slower compared to isotropic etching (e.g. the etch rate for a <100> silicon wafer immersed in KOH is 1µm/min at 80˚C). Commonly used anisotropic etchants are potassium hydroxide (KOH), ethylene diamine pyrocatechol (EDP) and tetra methyl ammonium hydroxide (TMAH).

### *1.1.3 Thesis Outline*

This thesis is organized as follows. The basics of micro-fabrication and the purpose of this research have already been covered in this chapter. A review of different techniques and trends in the fabrication of micro-needles, and the fabrication procedure implemented in this thesis are discussed in chapter two. The chapter describes the dimensions,

configuration and process schematics required for the desired micro-needle design. Chapter three presents a brief discussion about photo-mask generation and lithography. Here, the different resist tones, etching and lift off procedures are reviewed. The details regarding buried channel fabrication comprises chapter four. Both wet and dry etching techniques used to create the channels and inferences from the two etching methods are shown here. Chapter five comprises of the fabrication of the micro-needle body. This chapter also details the use of wet and dry etching processes to develop the needle body and the results inferred from them. Finally, the thesis ends with conclusions and scope for future work in chapter six.

# CHAPTER 2 LITERATURE REVIEW AND RESEARCH PLAN

## 2.1 Literature Review

Currently, transdermal fluid transfer typically involves a conventional syringe technique administered by authorized medical staff or trained personnel. This technique is inconvenient, painful, expensive, and potentially unsafe due to infections it may cause, and is time-consuming and unpleasant for long-term monitoring treatments.

Microfabrication techniques, originally developed for the microelectronics industry, provide a number of advantages over other technologies because they can deliver devices and structures that are small, reliable and inexpensive. A multitude of microchannels and reservoirs are readily integrated on a single chip, enabling parallel chemical analysis and leading to reduced cycle time. Miniaturized components will also enable rapid reaction rates, reduce material costs, and extract information from small samples. Microneedles can be defined to penetrate only the outermost layer of skin, which contains no nerve endings, thus avoiding inducing pain, and with reduced diameter, the holes they produce could be small enough to exclude bacteria, eliminating a potential source of infection.

Recent years has shown a continual effort and increased interest by researchers to produce high quality micro-fabricated needles. Fabricating micro-needles with materials that offer good resistance to buckling, bending and shear forces while also having the ability to delivery fluids effectively have been the main concern of most of the ongoing research.

There are basically two types of microneedles, in-plane and out-of-plane. Needle formation techniques include silicon wet and dry bulk micromachining, silicon surface micromachining, wafer bonding, etc. This section describes some of the key micro-needle designs that have been fabricated thus far.

### *2.1.1 Out of Plane Microneedles*

Out-of-plane microneedles refer to microneedles protruding vertically out of the base material.

**Prausnitz et al**

Prausnitz and his colleagues, at the Georgia Institute of Technology, were among the first to fabricate arrays of very short "painless" microneedles with microfabrication technologies use predominantly for the fabrication of integrated circuits (IC) [14]. They first fabricated an array of short, out-of-plane solid silicon microneedles using $SF_6/O_2$ reactive ion etching (RIE). This array was then used as a template to form a SU-8 epoxy mold covering the entire array, leaving the tips exposed. The mold was then partially filled with NiFe and the electrochemical process yielded hollow microneedles that were 150 μm in height with a base diameter of 50 μm and 100 μm spacing between them (Figure 2.1). Since the needles are short, they cross the stratum corneum without penetrating deep enough to stimulate the pain causing nerve. The array of micro-needles created by this process is suitable for drug patches but offer inadequate design flexibility for other applications.

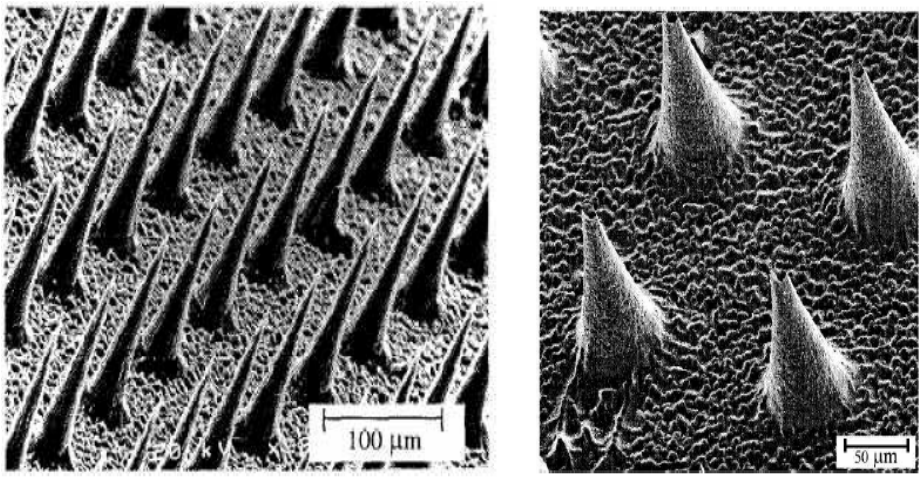


Figure 2.1: Out of plane silicon micro-needles [14]

**Gardeniers et al**

Gardeniers et al presented a fabrication procedure that used both anisotropic wet etching and directional dry etching techniques to obtain out-of-plane hollow microneedle structure arrays for transdermal fluid transport [15]. Figure 2.2 (Left) shows the microneedle fabrication sequence. The flow channel was etched using $SF_6$ plasma chemistry in RIE on a silicon substrate in the ‹ 100 › plane. The desired needle was 350 µm high with a base width of 250 µm and maximum width of the hole as 70 µm, and the flow channel was placed 40 µm from the tip. A slot as deep as the needle length and another channel connecting the flow channel through the backside of the wafer but with a varied cross-section, were also etched using the same RIE process. The inner surfaces of the holes and the slots were coated with a conformal layer of 500 nm of low stress silicon nitride using the LPCVD method to prevent the sidewalls from being etched in KOH, and the protective layer was stripped from the surface using directional $SF_6$ plasma. Anisotropic wet etching in KOH followed by immersing the needle array in a bath of 50% HF solution resulted in the needle structure shown in Figure 2.2 (Right).

The ramp structure leading to a sharp tipped needle was formed due to the slow etching of KOH in the ‹ 111 › plane of the silicon substrate. Even though out-of-plane fabrication processes yield uniformity of microneedles across the wafer with high needle density per chip, the length of the needles are usually limited by the mold or etch depth.

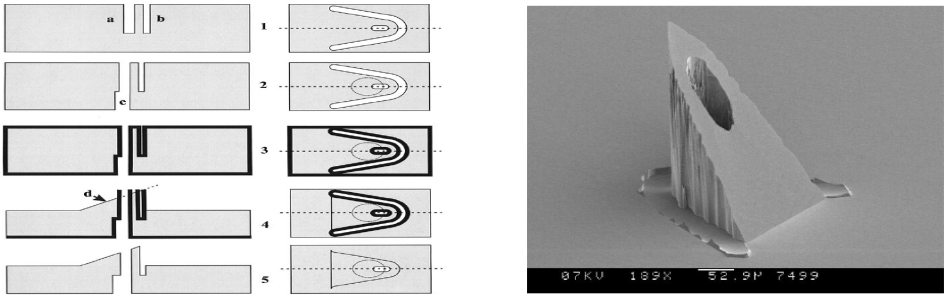


Figure 2.2: [Left] Fabrication process schematics for Gardeniers et al; [Right] Out of plane hollow microneedle [15]

### *2.1.2 In-Plane Microneedles*

In-plane microneedles refer to microneedles with shaft aligned parallel to the plane of the base wafer.

**Liwei Lin et al**

Lin created in-plane microneedles that had a silicon nitride microshell as the flow passage to conduct fluid along the length of the microneedle, on a silicon substrate, using a combination of surface and bulk micromachining techniques to create the microneedles [16]. The wafer was selectively doped to a depth of 12 μm with boron to provide an EDP etch stop as well as a mechanical support for silicon. PSG was used to create a sacrificial spacer layer with a thickness of 8 μm and a 2.5 μm thick silicon nitride shell was deposited over the sacrificial layer.
The microchannel was opened when this layer was etched in a bath of concentrated HF. The silicon substrate was thinned from the backside to 120 μm using a timed EDP etch. Further patterning steps and an etching in EDP both on the front and backside reduced the support layer to 50 μm while simultaneously releasing the needles, but keeping them anchored to the handle wafer. The needles were then separated mechanically from the handle wafer. Polysilicon line heaters were incorporated for bubble pumping fluid down the shaft of the microneedle, yielding sharp and functional microneedles. The schematic of the fabrication process and the close-up of the microneedle tip and cross-section of the microchannel are shown in Figure 2.3 and 2.4 respectively.

A few drawbacks of the needles produced by this method were that the silicon nitride microshell used for fluid transportation did not prove to be completely mechanically robust. So, the EDP etch, done to release the needles, had to be closely timed as longer EDP etch times resulted in blunt micro-needle tips.

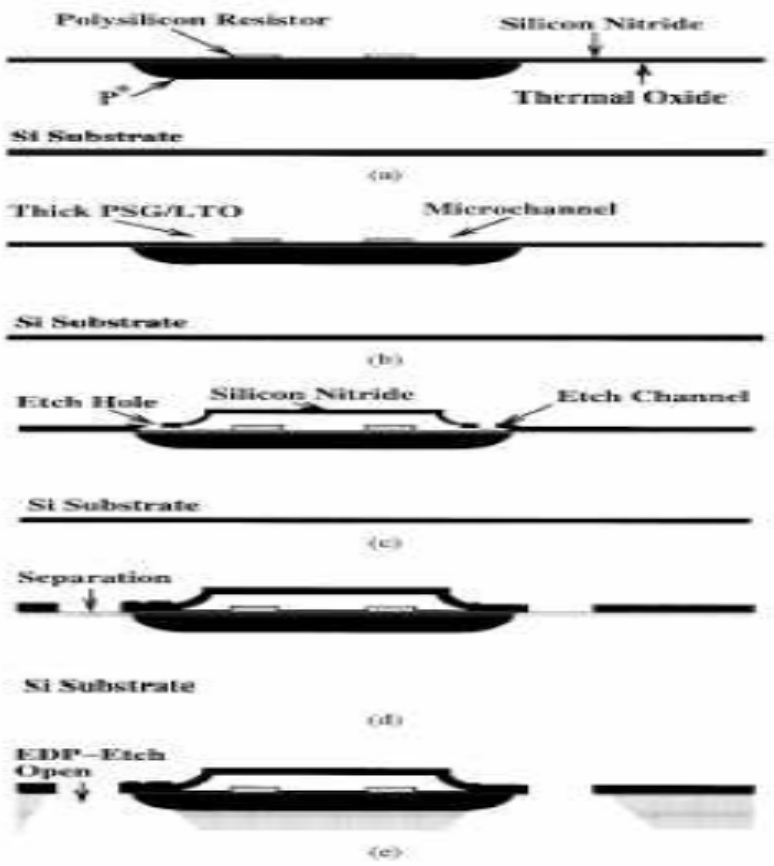


Figure 2.3: Steps involved in the fabrication process for Lin et al [16]

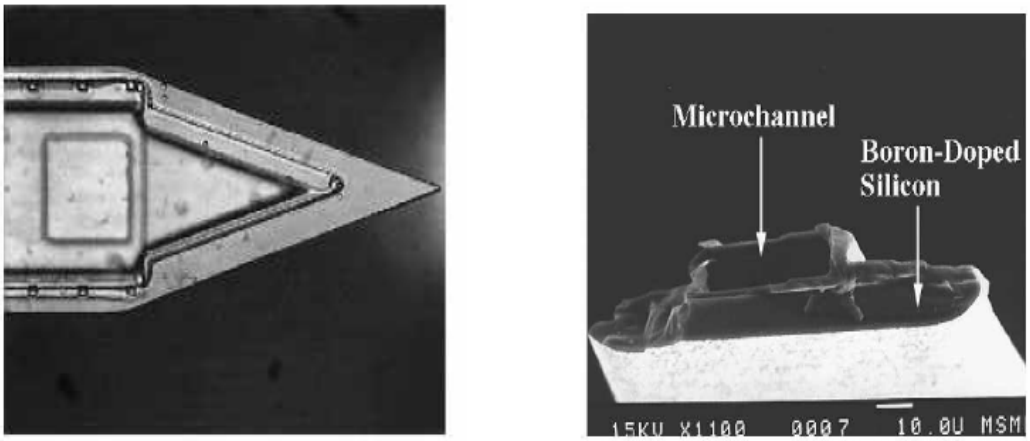


Figure 2.4: [Left] Top view of needle and reservoir; [Right] View of cross-section of microchannel [16]

**Parker et al**

Recently researchers at the University of California, Santa Barbara, fabricated in-plane bulk titanium microneedles with embedded microfluidic networks, using high aspect ration titanium micromachining and multi-layer lamination technologies [17]. Figure 2.5 shows the bulk titanium microneedle fabrication process flow. Here, a $TiO_2$ masking layer was sputter coated on both sides of a 25 μm thin chemically mechanically polished (CMP) titanium foil followed by an oxide patterning of the needle array, on the front, using $CHF_3$ dry etching process. A second lithographic step was used to partially transfer the embedded microfluidic network geometry onto the masking oxide. The $Cl_2$/Ar chemistry in bulk titanium etching was used to etch staggered microfluidic channels approximately half way into the titanium foil, and the remaining masking oxide was cleared using an oxide etch.

After the channels were defined using the titanium deep etching process, the foil was sputter coated with a 0.5 μm thin layer of gold. The channels were sealed by bonding this foil with another foil, also coated with 0.5 μm of gold, by the thermo compression process. The $TiO_2$ film on the backside of the foil was used as a mask to through etch the bottom foil to obtain the needles as shown in Figure 2.6. Needles with 10 μm long and 25 μm wide fluid ports, different tip angles of 15˚, 30˚ and 45˚, and varying shaft lengths of 500 μm, 750 μm and 1000 μm were fabricated. This approach combines the benefits of bulk micromachining with the toughness of titanium to produce robust microneedles at a low cost. However, there is a possibility of wafer-to-wafer misalignment during bonding processes.

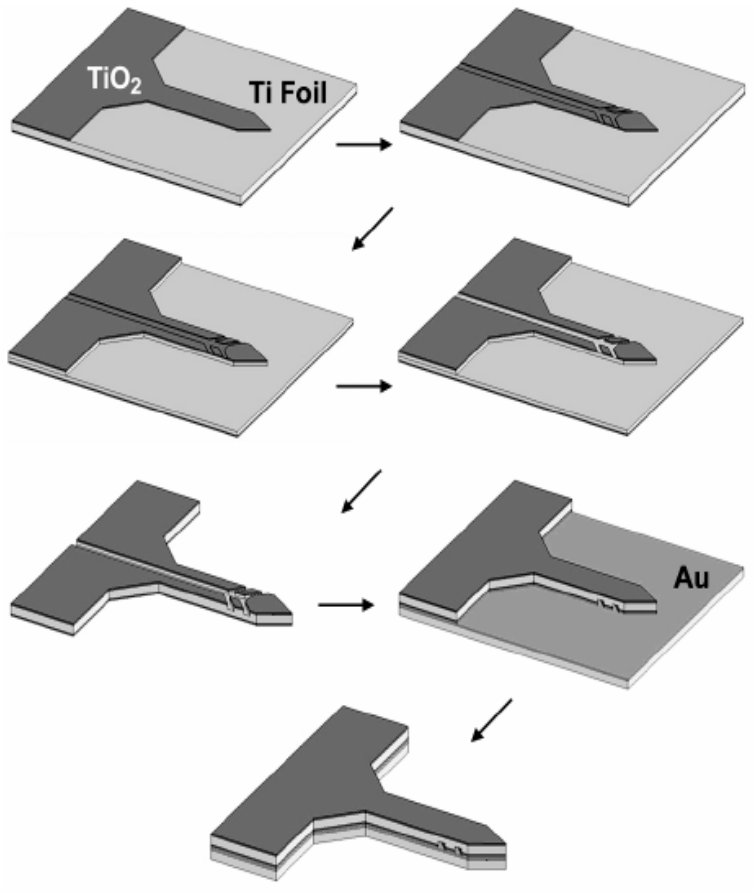


Figure 2.5: Process flow for fabrication of bulk titanium micro-needles [17]

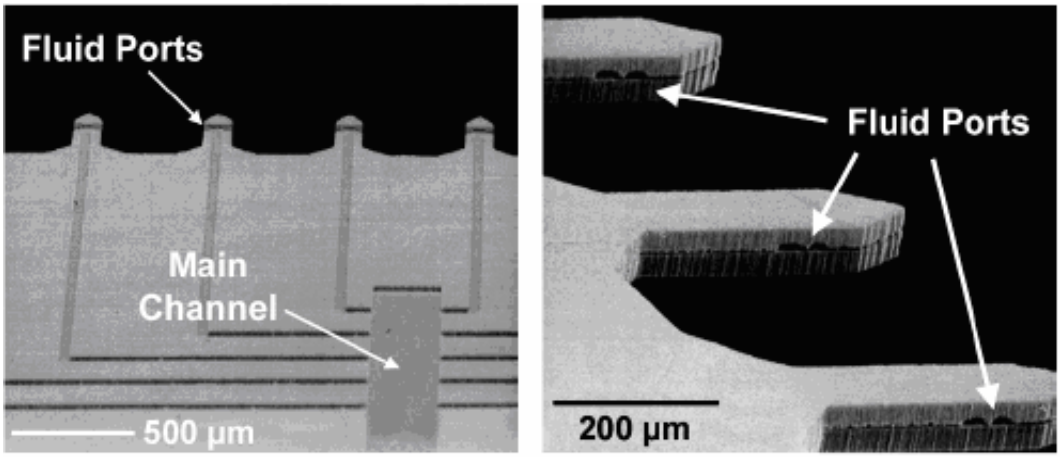


Figure 2.6: Scanning electron micrographs of [Left] embedded microfluidic networks before bonding; [Right] fluid ports on the side [17]

### *2.1.3 In-Plane Microneedles with Buried Channels*

**Boer et al**

Reference [19] presents a fabrication method called the "buried channel technology" (BCT) for fluidic applications such as channels, cavities and connectors in silicon wafers. This paper describes four different process schemes that can be used to create micro-channels on a ‹ 100 › silicon wafer. The altered methods and the steps involved in constructing the channels are shown in Table 2.1.

Boer et al also describes how different channel shapes (Figure 2.7- Left) can be created by varying the trench depth and types of etchants used for the buried structures. Channels of hemi-circular shape at the surface of the substrate (Figure 2.7-1), circular bulk (Figure 2.7-2), V-groove bulk (Figure 2.7-3) or V-groove structures at the surface (Figure 2.7-4) can be fabricated by using a few or all of the steps described in Table 2.1. For the V-groove structures, the silicon wafer was anisotropically etched in the ‹ 111 › plane. The size of the groove was adjusted by an additional step involving deep reactive ion etching (DRIE) of the ‹ 110 › plane of the silicon substrate. Figure 2.7 (Right) is an example of a circular channel etched electrochemically in a 5% aqueous HF solution.

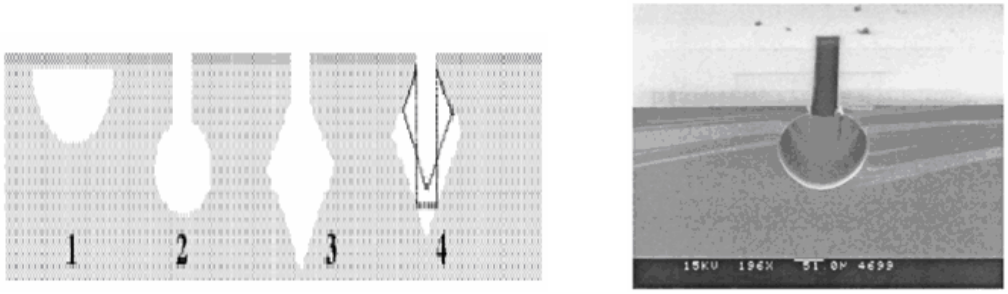


Figure 2.7: [Left] Different shapes of micro channels (1) Hemi-circular at surface; (2) Circular in bulk; (3) V-groove in bulk; (4) V-groove at surface; [Right] Circular channel etched electrochemically in 5% aqueous HF solution [19]

**Table 2.1: Process schemes for BCT [19]**

| Step nr. | Scheme 1<br>(Isotropic-Dry)<br>RIE | Scheme 2<br>(Isotropic-Wet)<br>Electrochemical HF | Scheme 3<br>(Isotropic-Wet) $HF/HNO_3/H_2O$ | Scheme 4<br>(Anisotropic-Wet) KOH |
|---|---|---|---|---|
| Substrate specifications | p or n-type silicon<br>resisitivity not critical<br>crystal orientation not critical | p-type silicon<br>resisitivity 0.01-10 ohm.cm<br>crystal orientation not critical | p or n-type silicon<br>resisitivity not critical<br>crystyal orientation not critical | p or n-type silicon<br>resisitivity not critical<br>anisotropic etching {100}, {110} |
| 1: Mask material | Thermal $SiO_2$ + Cr | LPCVD of $Si_3N_4$ + Cr | LPCVD $Si_3N_4$ + Cr | LPCVD $Si_3N_4$ + Cr |
| 2: Pattern transfer | Lithography,RIE-$CHF_3$ | Lithography,RIE-$CHF_3$ | Lithography,RIE-$CHF_3$ | Lithography,RIE-$CHF_3$ |
| 3: Protection of coating layer | 1.Underetch DRIE<br>2. Isotropic pre-etch<br>3. SLE-etch | 1. Isotropic pre-etch or<br>2. SLE-etch | 1. Isotropic pre-etch 2. SLE-etch | 1. Isotropic pre-etch<br>2. SLE-etch |
| 4: DRIE of the trench | Cryogenic ICP-$SF_6$ plasma | Cryogenic ICP-$SF_6$ plasma | Cryogenic ICP-$SF_6$ plasma | Cryogenic ICP-$SF_6$ plasma |
| 5: Coating of the trench | Thermal $SiO_2$ | LPCVD $Si_3N_4$ | LPCVD $Si_3N_4$ | LPCVD $Si_3N_4$ |
| 6: Etching of the coating at the bottom of the trench | RIE-$SF_6$ | RIE-$SF_6$ | RIE-$SF_6$ | RIE-$SF_6$ |
| 7: Etching of the buried structures | Isotropic $SF_6$ plasma | Electrochemical etching in HF | $HF/HNO_3/H_2O$ | KOH |
| 8: Stripping coating | $SiO_2$ in HF, BHF | HF (50%) | HF(50%) | HF (50%) |
| 9: Filling of the trench | LPCVD of poly Si, $SiO_2$ or $Si_3N_4$ | LPCVD of poly Si, $SiO_2$ or $Si_3N_4$ | LPCVD of poly Si, $SiO_2$ or $Si_3N_4$ | LPCVD of poly Si, $SiO_2$ or $Si_3N_4$ |
| 10: Release of channels | $Si_xN_y$: KOH | $Si_xN_y$: KOH | $Si_xN_y$: KOH | $Si_xN_y$: KOH |

The methods described in reference [18] need only a single lithographic mask to fabricate the micro-channels and since the needles can be processed on one side of the wafer, the need for wafer-to-wafer bonding is eliminated.

**Chen et al**

Chen and his colleagues constructed neural recording arrays for selective chemical delivery, at the University of Michigan [13]. The microneedles were developed using a combination of buried channel and dissolved wafer processes, with silicon as the substrate.

The fabrication process is as shown in Figure 2.8. First, the wafer was heavily doped with boron, which acts as an etch stop, to a depth of 2 μm. For the flow passage, 2.5 μm trenches arranged as a row of closely fitted "chevron structures" (Figure. 2.9) along the length of the needle were etched through the doped silicon to expose the undoped silicon. Ethylene-di amine pyrocatechol (EDP) was then used to create the channel by ethching the undoped silicon at the bottom of the trenches.

Due to EDP's anisotropic etching capabilities, it etches slowest in the ‹ 111 › plane of silicon, thereby causing undercuts in the doped region and forming a continuous channel with bridges over it. The walls of the channels were then doped with boron to a depth of 15 μm and the wafer was thermally oxidized, causing a volume change and the bridges to expand and close the gap between them. The channel was completely sealed by adding a layer of oxide using low-pressure chemical vapor deposition (LPCVD). Wet isotropic silicon etching and EDP were used to release the needles.

This process is useful when electrodes and fluid flow passages need to be integrated onto the same microneedle with multiple chemical delivery and recording ports.

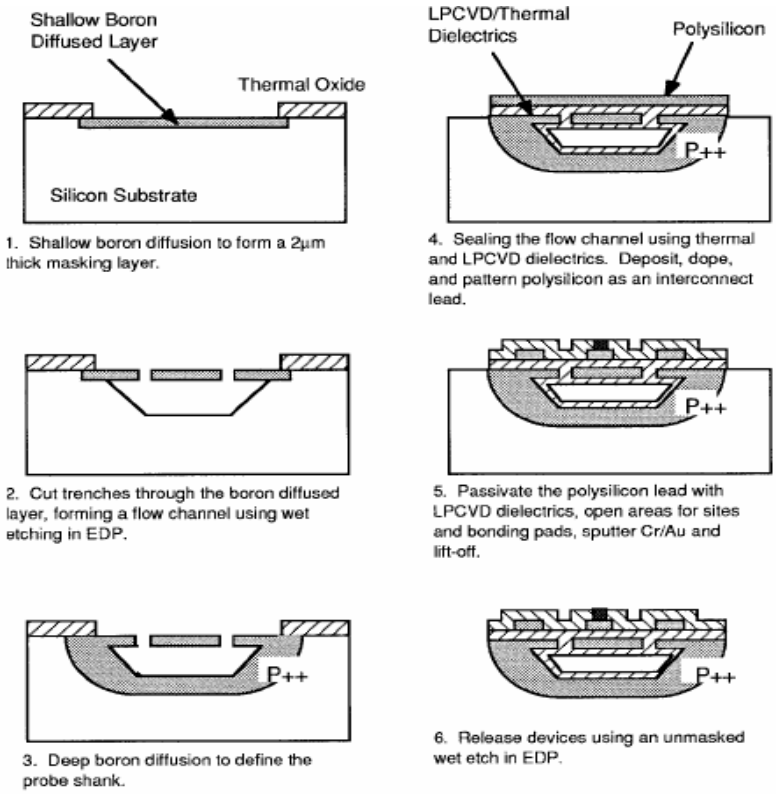


Figure 2.8: Fabrication steps involved in the process created by Chen et al [13]

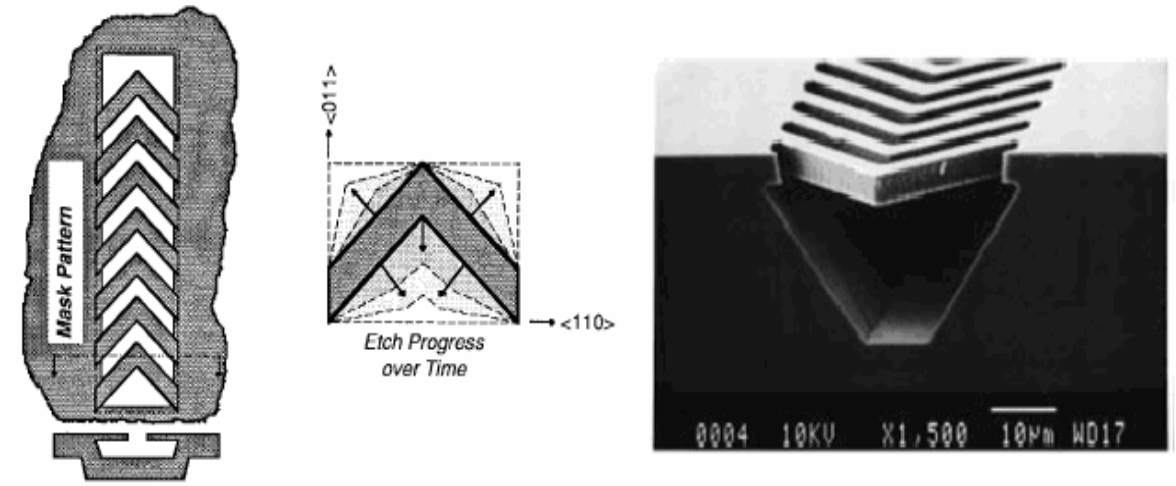


Figure 2.9: [Left] Closely fitted chevron structures over the channel; [Right] View of a cross-section of the etched microchannel [13]

**Paik et al.**

The initial research plan for designing microneedles of varying dimensions and tip taper angles (Table 2.2) in this thesis has been inspired by the in-plane single crystal silicon microneedles fabricated by Seung-Jun Paik and colleagues [18], using the process flow described by Figure 2.10. Microchannels were fabricated on a ‹ 100 › silicon substrate, deposited and patterned with $SiO_2$ etch mask on both sides, by a sequence of anisotropic dry etch followed by a coating the side walls of the etched surface with a passivation layer of thermal oxide or nitride using LPCVD. A circular channel with a diameter of 20 µm was isotropically dry etched with $SF_6$ plasma chemistry and the trench was filled with polysilicon using the LPCVD process. Deep silicon etching was used on the front side of the wafer to define reservoirs of 2 mm x 2 mm and the 100 µm thick needle shaft. The microneedles, of the same thickness as the wafer (550 µm), were released by using the same deep etching process. The released needles are shown in Figure 2.11.

Although these in-plane microneedles could be easily integrated with microfluid chip systems, experimental tests using the microneedles of different tip taper angles suggested that the 30˚ isosceles triangle tip was most robust during penetration and that needles with smaller tip angles of about 10˚ of less were not mechanically very stable.

**Table 2.2: Design variation in micro-needle shaft [18]**

| Type | Overall geometry | Shape of the tip | Tip taper angle (°) |
|---|---|---|---|
| A | 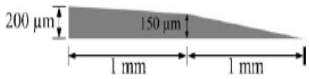  | Right triangle | 8.5 |
| B | 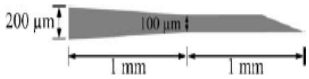  | Right triangle | 15 |
| C | 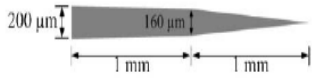  | Isosceles triangle | 9.5 |
| D | 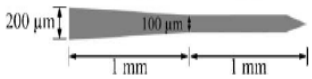  | Isosceles triangle | 30 |

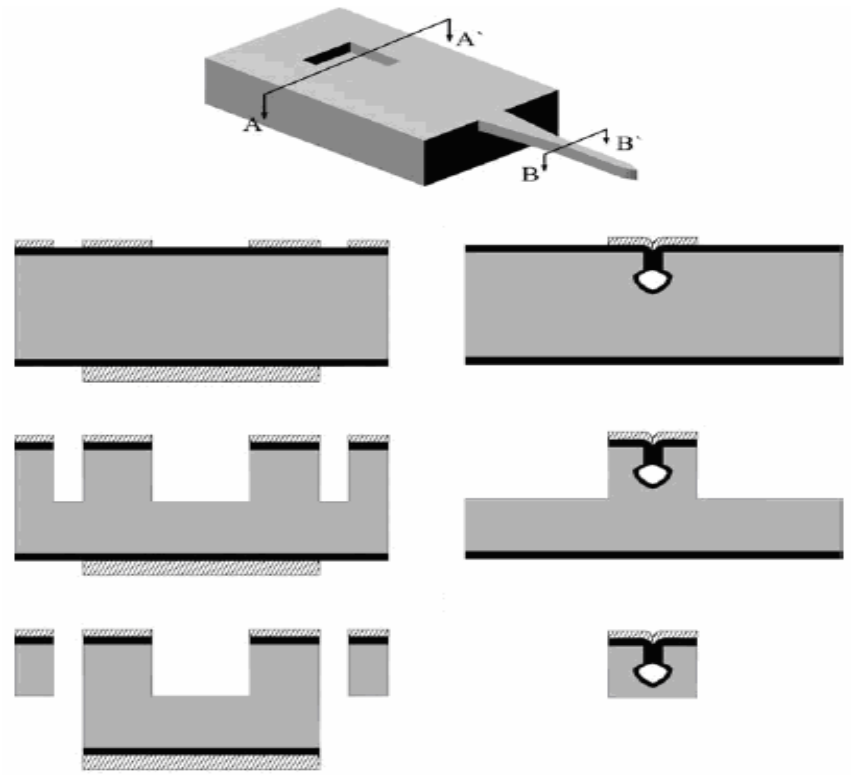


Figure 2.10: Schematic diagram of a micro-needle and fabrication process flow for cross-sections A-A′ and B-B′ [18]

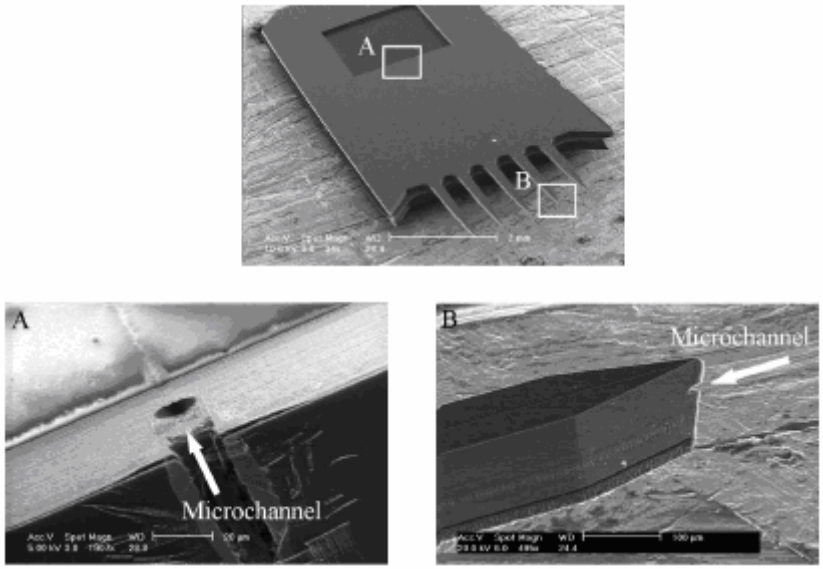


Figure 2.11: Scanning electron micrographs of [Top] fabricated micro-needle; [A] micro-channel entrance at reservoir; [B] micro-channel entrance at tip of micro-needle [18]

## 2.2 Research Plan

### *2.2.1 Micro-needle Design*

As mentioned in section 1.1, the purpose of the fabrication of microneedles in this thesis is to provide a medium for injecting minute amounts of transgenic virulent fluids, tagged with fluorescent markers, into the visual cortex of mice (Figure 2.12- Left). It is necessary to design the needle body and shaft in complete accordance to the limitations posed by the anatomical structures of the skull and the inner cavity. Since it is desirable to probe various locations of mice brain, a ramp-like design for the needles has been suggested (Figure 2.12- Right) to ensure that the fluid is released efficiently in the desired locations of the visual cortex.

The approximate thickness of a mouse's skull is 2 mm and the visual cortex lies at a depth of about 1 mm below the skull. Also, the preferred incision on the mouse skull is not to be more than 2 mm wide. Therefore, the total length of the needles has been fabricated at 3 mm, of which the dimensions of the shaft are 2 mm x 1 mm (length x width) and the length of the longest needle is 1 mm. Lastly, each needle, with a thickness of 200 μm, is placed at a distance of 100 μm from its neighboring needle to limit the damage incurred by the visual cortex at the time of insertion. Keeping in mind that the fabricated microneedle must finally also allow for ease of handling and integration with microfluidic systems, the needle body is designed to be 1 cm x 1 cm.

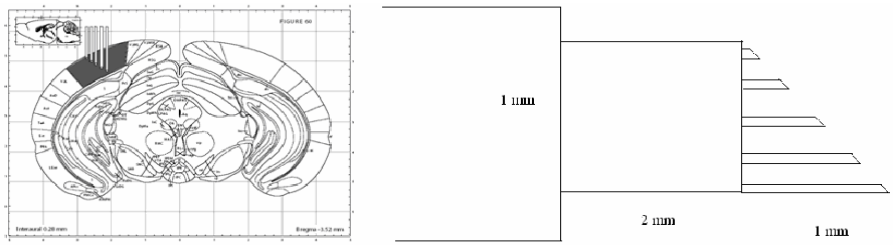


Figure 2.12: [Left] Graphic of micro-needle insertion into visual cortex of a mouse [Obtained from Dr. Botond Roska]; [Right] Schematic of needle proposed

In order to deliver the transgenic virulent fluid, having a viscosity of $\rho = 10^{-3}$ N s $m^{-2}$, into the visual cortex at the rate of Q = 100 pL $s^{-1}$, a narrow rectangular microchannel of width a = 4 μm, height b = 20 μm and length L = 6000 μm is assumed. The pressure drop, ΔP, across the channel is given by [20]

$$\Delta P = \frac{8\rho LQ}{\pi D_H^4}$$

Equation 2.1

$D_H$ is the hydraulic radius and is given by [19]

$$D_H = \frac{2(ab)}{(a+b)}$$

Equation 2.2

Substituting for the appropriate values in Equations 2.1 and 2.2, the pressure drop across the channel is about 2.3 x $10^{-10}$ N $m^{-2}$.

The fluid encounters frictional resistance, f, from the walls of the channel, directly proportional to the total length that it travels and inversely proportional to the hydraulic radius of the channel (Equation 2.3)

$$f \propto \frac{L}{D_H}$$

Equation 2.3

Since the frictional resistance is inversely proportional to the hydraulic resistance, which is a function of the width and height of the channel (Equation 2.2), reservoirs each of 100 x 100 μm have been constructed larger than the channel width of 4 μm, so that there is minimal resistance to the fluid being pumped through the channel. Frictional resistance in the channel is much more than that experienced in the reservoir, making sure that the fluid arrives at the outlet with the desired flow rate. The channels are placed at a distance of 10 μm from the tip of the needle (Figure 2.13) to avoid the blockage of the opening

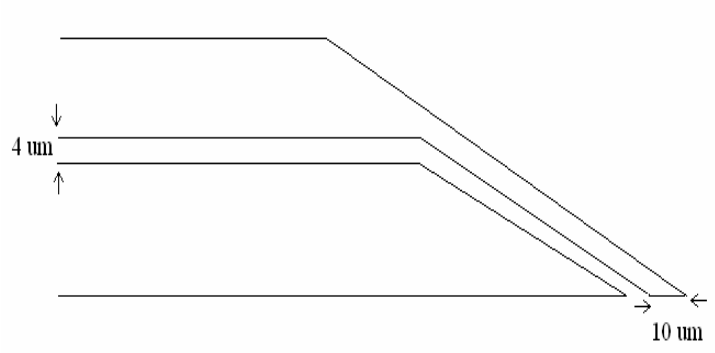


Figure 2.13: Schematic of the micro-channel in the needle proposed

during needle insertion and render adequate transmission of the injected molecules into the point of interest.

### *2.2.2 Mask Material*

The needle bodies and channels are etched on a 4 inch one-side polished ‹ 100› oriented p-type silicon substrate using DRIE. To successfully transfer patterns onto silicon, it is essential to find a masking material that can withstand etching process so that the desired Si area can stay and be removed easily afterwards.

DRIE is a plasma-based highly anisotropic process which also involves bombarding the substrate with extremely energized ions. Silicon, being a brittle metalloid, cannot withstand the force with which the ions hit the surface and may thus crack and crumble. So, the wafer needs to be layered with a suitable mask that can withstand the chemical and physical reactions from the plasma for the entire duration of the etching process. Also, the etch rate of the masking material must be much lower than that of the substrate under the same process conditions. On experimenting with various materials, it is observed that aluminum is the most appropriate mask metal for this purpose. Here, the silicon substrate is sputter coated with a 1000 Å thick layer of aluminum mask. Moreover, the non-reactive and non-catalytic characteristics of aluminum towards $SF_6$

and $CHF_3$ gases as well as the easy availability of the metal make it the most sought after choice as the masking material [21]. Since the Si/Al selectivity is high, the Al film sufficiently protects the unexposed silicon substrate while allowing a 60 μm deep trench to be etched with the $SF_6/CHF_3/O_2$ plasma. Furthermore, the aluminum mask can be easily stripped off from the released needles using an aluminum etchant.

### *2.2.3 Fabrication Process*

The steps involved in producing the microneedle channels are as described in Figure 2.14. For the fabrication of the channels, positive photo-resist (AZ 5214) is spun on the wafer at 3500 rpm for 30 seconds. The process of image reversal is performed in order to obtain a high resolution negative resist [10]. This is followed by transferring the desired pattern onto the wafer using standard photolithographic techniques. The wafer is then subjected to DRIE, using a modified Bosch process, explained in section 4. The anisotropic etching properties of the DRIE are used to etch vertically down into the wafer up to 40 μm, after which a 20 μm deep circular channel is isotropically scalloped. After stripping the wafer of any remaining photo-resist with acetone, the channels thus fabricated are then sealed with $SiO_2$ at the rate of 1 μm/minute, using PECVD. Buffered hydrogen fluoride (BHF) can be used to remove surplus $SiO_2$.

The needle bodies are fabricated (Figure 2.15) by using electron beam evaporation (EBE) to deposit a 1000 Å of aluminum on the wafer. The image is transferred onto the mask after coating it similarly with positive photo-resist. The aluminum is then removed from the non-structural areas of the wafer using an aluminum etcher. After eliminating the remaining photo-resist using acetone, the standard Bosch process (also explained in section 4) of the DRIE is used to release the needles. The final objective is to be able to create the micro-needles that can be integrated to an external robotic fluid pumping system as shown below in Figure 2.16.

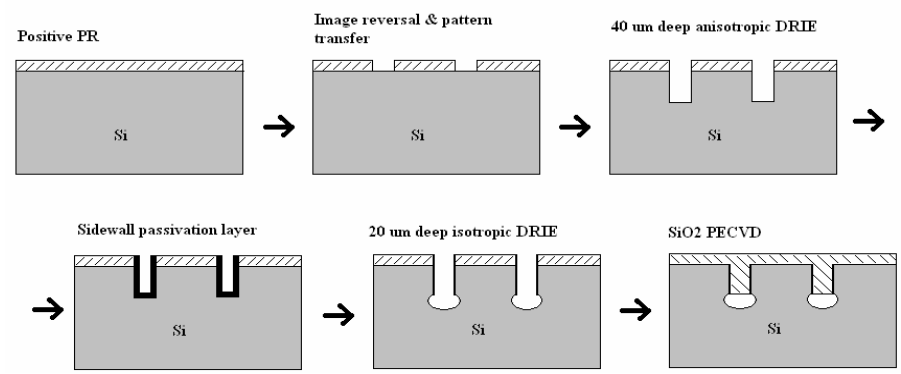


Figure 2.14: Process flow for the fabrication of the micro-channels

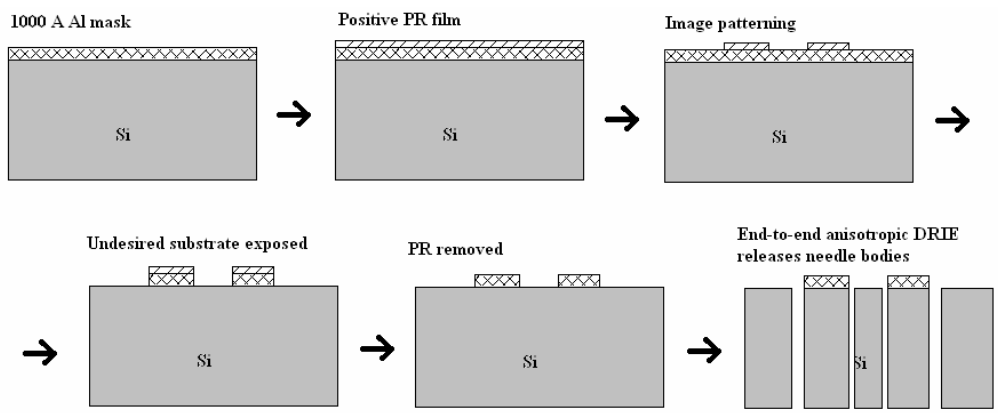


Figure 2.15: Process flow for the fabrication of the micro-needle body

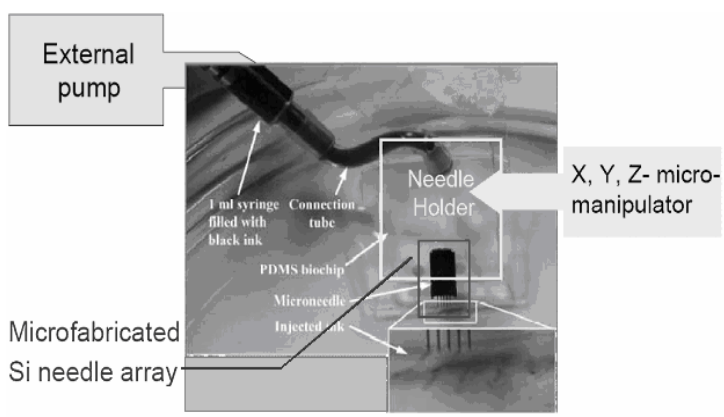


Figure 2.16: Example of integrated microneedle microfluid chip [18]

# CHAPTER 3 PHOTOMASK GENERATION AND LITHOGRAPHY

## 3.1 Photomask

The photomask is an optical master template made from highly polished fused silica and coated on one side with an absorber material, such as chromium, and a photoresist layer [22] [23]. The standard size of a photomask is 5.0 in x 5.0 in x 0.09 in [21]. In creating a photomask, first the desired pattern is built using any software tool designed for mask layout. Here, the Layout Editor, L Edit (version 11.1) has been used to engineer the required layout for the mask. Figure 3.1 shows a screen view of one of the proposed microneedle designs, created using L Edit. After the preferred shapes have been established thus, they are converted into a format suitable for use by a pattern generator; in this case, the GCA/ David W. Mann Pattern Generator 3000 and etched onto a thin glass plate called the reticle. The reticle must be capable of transferring the pattern image accurately onto the photomask, since the photomask serves as the master copy for all subsequent pattern exposures.

Following the etching of the pattern onto the reticle, the reticle is used to replicate the image onto the chromium layer of photomask plate, and the photomask is developed. When a photomask is used to transfer the pattern onto a wafer through contact printing, the photo emulsion side of the plate is pressed against the photoresist side of the wafer. Since this type of pattern transfer takes place many times, continual use of the photomask degrades the photo emulsion layer. Hence, chromium is used as an optical masking material due to its endurance to physical contact and optical density exposure [21]. Also, since there must be symmetry between the patterns on the photomask and the wafer, the photomask is made of amorphous fused silica as it possesses desirable characteristics like high transmittance and low reflectance at the wavelength of the wafer exposure tool [21].

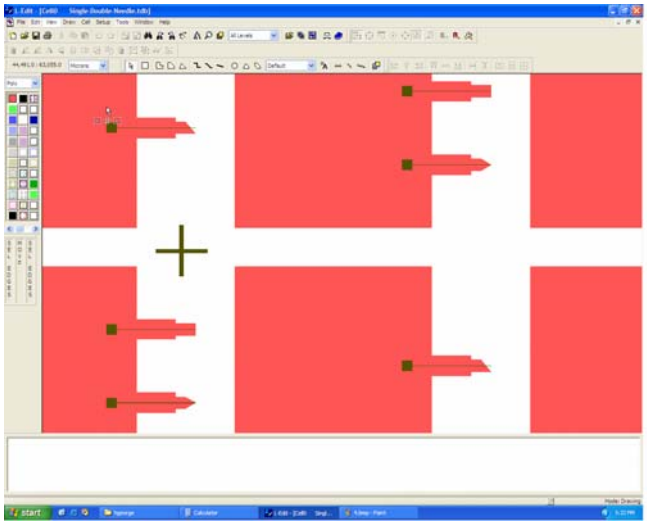

Figure 3.1: Screen view of a proposed microneedle pattern designed on a layout editor, L-Edit (v11.1); the cross mark is patterned on the mask for alignment purposes

## 3.2 Photolithography

Microfabrication is based on the ability to faithfully transfer the image from a photomask onto a thin film coating i.e. photoresist, on the surface of the substrate. This can be achieved when UV light, collimated by a series of lenses, passes through the photomask onto the substrate and selectively exposes the photoresist. This process is called optical lithography or photolithography, and shares much similarity with photography. The exposure to the UV light induces cross-links in the polymeric photoresist, which will remain as the image pattern is developed on the substrate and act as a mask material for subsequent etching.

Photolithography typically includes the following steps. First, the wafer is chemically cleaned by the RCA cleaning process to remove any particulate matter on the surface as well as any traces of organic, ionic or metallic impurities. The RCA cleaning process has three major steps that are used in sequence; the insoluble impurities are first removed with a 5:1:1 $H_2O$: $H_2O_2$:$NH_4OH$ solution, followed by the removal of metallic

contaminants using a solution of diluted HF, and finally the ionic impurities are gotten rid of with a solution of 6:1:1 $H_2O$: $H_2O_2$: HCl.

The wafer is then heated for a minute at about 90˚C to drive away any moisture that may be present on its surface. Hexamethyl disilizane (HMDS) is applied on the wafer in liquid or vapor form to promote adhesion of the photoresist. The photoresist is coated onto the wafer using a spinner whose spin rate determines the thickness of the photoresist layer desired. This is followed by a soft-bake of the wafer at 90˚C for a minute to remove excess solvent. After this, the wafer is placed under the exposure system for the pattern transfer. The contact printer, Cobilt A800 Mask Aligner COB C.5, was used for this purpose.

The exposure step is followed by a post exposure bake to reduce the effects of constructive and destructive interference patterns of light from the exposure. The resist is then developed in an alkaline metal-ion free (MIF) developer, such as tetra-methyl-ammonium-hydroxide (TMAH), which removes the exposed or unexposed areas of the photoresist depending on the resist tone used. After developing, the wafer is hard-baked for two minutes at 120˚C to solidify the remaining photoresist, which serves as a protective layer during the etching process.

Figure 3.2 summarizes the steps involved in the photolithographic process. The developed patterns, on the left and right, display characteristics opposite to each other. The figure uses different tones (positive and negative) of photoresist to illustrate some finer points in photolithography. This will be explained in the following.

### *3.2.1 Photoresist*

Photoresist is a combination of a polymer, a sensitizer and a casting solvent [10]. Photoresists are classified into positive and negative based on the resist tone, which

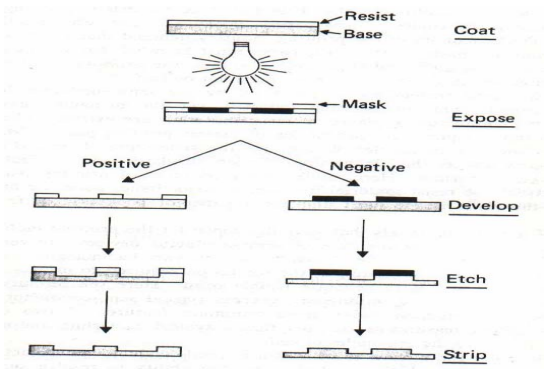

Figure 3.2: Schematic of photolithographic process [24]

depends on how the polymer structure changes on exposure to UV radiation. The reactions in the polymeric phase are controlled by the sensitizer, while the casting solvent enables the resist to be coated on the wafer in thin layers using spin-coating techniques.

Positive tone resists are used when the region of the wafer that is exposed to the UV light needs to be removed. Exposure of this type of resist changes the chemical structure of the polymer such that it becomes more soluble in the photoresist developer. Polymethyl methacrylate (PMMA) is an example of positive photoresist. Alkaline solutions such as KOH and TMAH can be used to develop resists of this tone. Contrary to positive photoresists, exposure of negative resist to UV light causes the resist to polymerize, thereby making it relatively insoluble in the developer. Figure 3.3 gives a schematic of the results obtained by the use of positive and negative resist tones. AZ 327 MIF developer, containing 5% TMAH in combination with a surfactant such as water, and that can be used with all AZ photoresists has been used to develop the required patterns of the microneedle bodies and channels.

### *3.2.2 Image Reversal*

Image reversal (Figure 3.4) of certain positive tone photoresists is done to obtain a high resolution negative tone material, to overcome the swelling that most of the negative

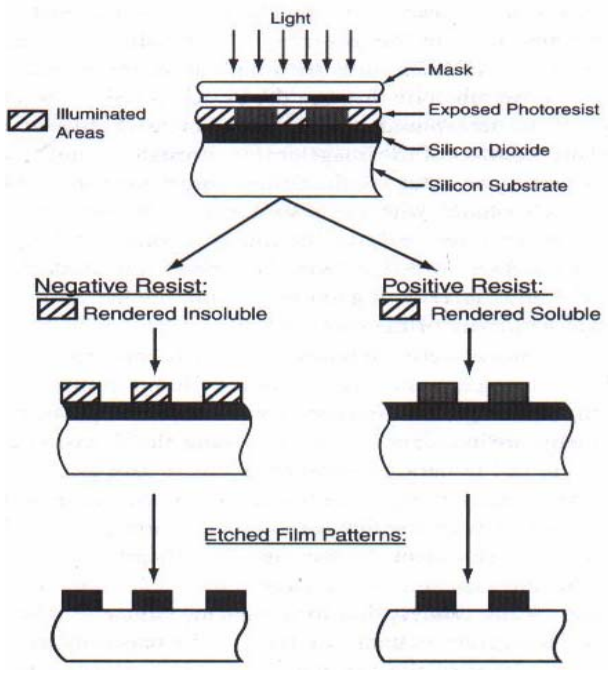


Figure 3.3: Schematic of results obtained by positive and negative photoresists [10]

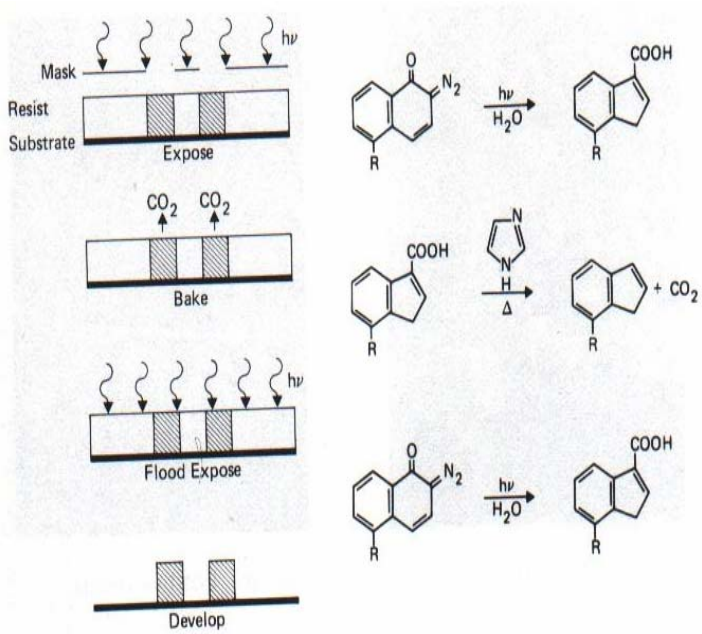


Figure 3.4: Process sequence for image reversal in a positive photoresist [24]

photoresists exhibit. To obtain a negative image through the process of image reversal, the substrate is first coated with a diazo amine positive photoresist and exposed through a mask, causing the amine vapors to diffuse into the exposed areas. The wafer is then baked, leading to the photodecomposition of the resist. The amine neutralizes the bi-product of the photodecomposition and renders the exposed areas insensitive to further exposure or development. This is followed by a flood exposure to make the areas adjacent to neutralized image soluble in conventional positive photoresist developers, resulting in a negative image of the mask with an undercut profile. The undercut profile is desirable as it allows for lift-off of film layers coated through evaporation or sputter mechanisms. Image reversal of certain negative photoresists such as KTFR is also possible [10]. AZ 5214, a positive photoresist, ideally made for image reversal, has been used to pattern the microneedle channels on the wafer.

### *3.2.3 Lift – off*

Lift-off is an additive process that is used to remove metals that are otherwise difficult to etch with plasma [23]. As shown in Figure 3.5, in this process, the wafer is coated with a layer of photoresist, patterned and developed. Metal films can be deposited on the developed wafer by sputter or evaporation mechanisms. Baking the wafer prior to film deposition is done to remove any excess solvent since photoresist tends to outgas slightly in vacuum systems, thereby degrading the film quality [25]. However, the time and temperature for which the wafer is baked must be moderate to avoid overflow of resist.

The desired metal film is deposited over the substrate, covering the areas containing the photoresist as well as places where the resist has been removed. During film deposition, care must be taken to ensure that the substrate does not reach temperatures high enough to burn the photoresist. Also important is that metal atoms deposit onto the substrate in one direction i.e., non-conformal coating as in evaporation, rather than from all the

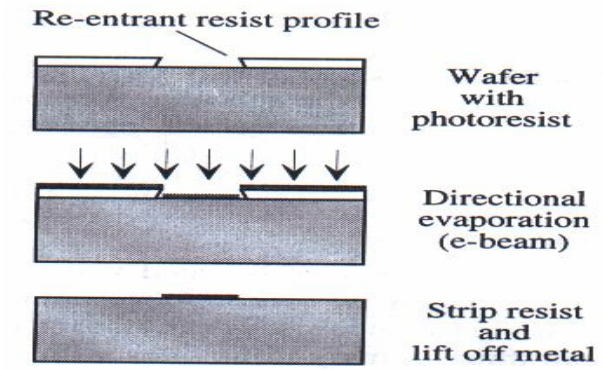


Figure 3.5: Lift-off sequence with positive photoresist [24]

directions, such as conformal coating by sputtering. The above two conditions (non-conformity and low temperature) can be satisfied by metal deposition.

This step is followed by immersing the wafer in a bath of photoresist solvent, such as acetone. The solvent removes the photoresist, which in turn takes the film along with it, leaving only the film that has been deposited directly on the substrate. Depending on the robustness of the metal film, the wafer may be required to soak in the solvent for a longer time.

### *3.2.4 Alignment Marks*

For most miniaturized devices having various differently patterned thin film layers stacked one on top of another, it is necessary to align consecutive layers with a previously patterned layer. Inclusion of fiducially placed marks called alignment marks on the first as well as each progressive mask, as needed, ensures accurate line up of layers. Double-sided wafers can also be used for precise stacking of layers. In this case, cross hair marks can be placed on the masks and the double-sided wafer can be inserted between two masks after aligning the first mask to the second one, followed by UV exposure simultaneously on both sides of the wafer (Figure 3.6).

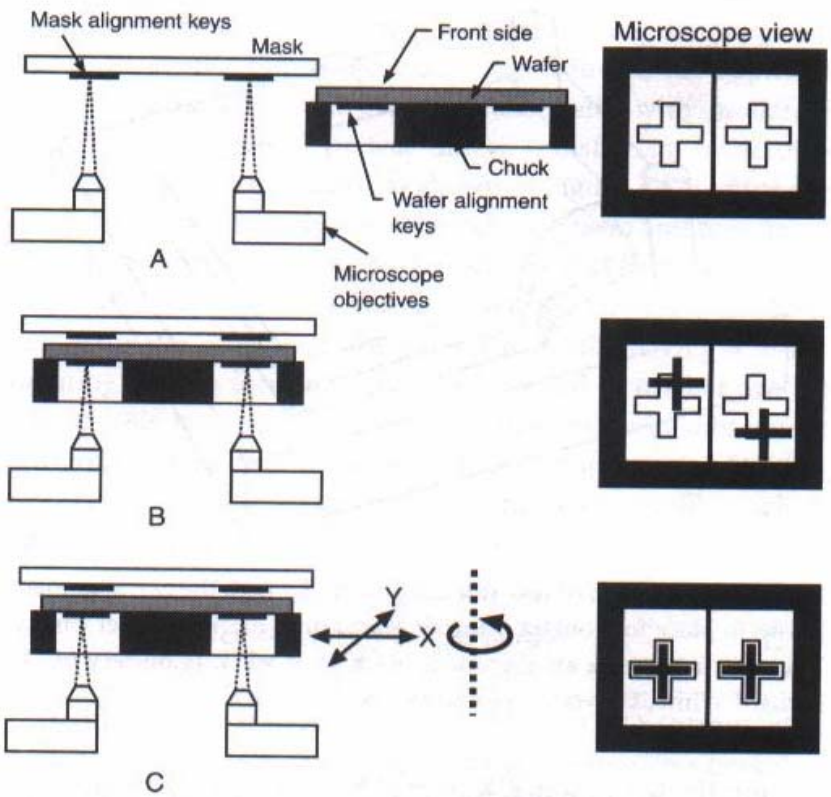


Figure 3.6: Double sided alignment scheme; (A) image of mask alignment marks electronically stored; (B) focusing of alignment marks on back side of wafer; (C) position of wafer adjusted to align marks to stored image [10]

# CHAPTER 4 BURIED CHANNEL FABRICATION

## 4.1 KOH Etching

### *4.1.1 Silicon Structure*

The crystal structure of silicon is similar to that of diamond [27]. The three most important crystallographic planes of the silicon structure usually taken into consideration are {100}, {110} and {111}. The bond structure of the atoms arranged in the <100> and the <110> directions are such that atoms with two bonds are directed into the crystal lattice while two valence bonds remain free; whereas, the Si atoms arranged in the <111> direction have three bonds directed into the lattice and only free bond, making the atoms in this plane more stable when compared to atoms in the (100) and (110) planes [23] (Figure 4.1).

The closely packed atom structure in the {111} planes makes etching using strong bases in the <111> direction much slower than in the <100> or <110> directions [23]. The angles formed between the different planes {100} and {110}, {100} and {111}, and {111} and {110} are 45° or 90°, and 54.7° or 125.3°, and 35.3° or 90° or 144.7°, respectively, at these intersections [27].

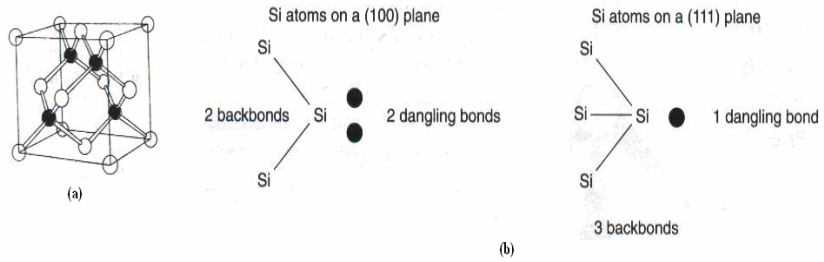


Figure 4.1: Arrangement of atoms in the (a) silicon crystal lattice; (b) (100) and (111) planes [10]

### *4.1.2 Anisotropic Wet Chemical Etching*

Wet chemical etching involves the removal of unwanted materials from the substrate by the use of certain acids or bases, by dissolving the reaction products in the chemical solution or by carrying them away from the desired structure [28]. Two most commonly used strong-base wet chemical etchants are KOH and EDP [10]. The steps included in the anisotropic etching process summarized by reference [10] are as shown in Table 4.1.

In this mechanism, the patterned wafer is immersed in a solution formed by dissolving a certain percentage by weight of KOH pellets in water. The overall reaction that takes place between the material to be removed and the OH ions is as shown [30]

$$Si + 2OH^{-} \rightarrow Si(OH)_2^{++} + 4e$$
$$Si(OH)_2^{++} + 4e^{-} + 4H_2O \rightarrow Si(OH)_6^{--} + 2H_2 \qquad \text{Equation 4.1}$$

Hence, the dangling silicon bonds are broken by the insertion of the hydroxide ions to form Si $(OH)_4$ as shown [30]

**Table 4.1: Summary of process steps used in anisotropic wet etching [10]**

| Process | Duration | Process temperature (°C) |
|---|---|---|
| Oxidation | Variable (hr) | 900–1200 |
| Spinning resist at 5000 rpm | 20-30 s | Room temperature |
| Prebake | 10 min | 90 |
| Exposure | 20 s | Room temperature |
| Develop | 1 min | Room temperature |
| Postbake | 20 min | 120 |
| Stripping of oxide (BHF:1:7) | ± 10 min | Room temperature |
| Stripping resist (acetone) | 10–30 s | Room temperature |
| RCA1 [$NH_3$(25%) + $H_2O$ + $H_2O_2$:1:5:1] | 10 min | Boiling |
| RCA2 (HCl + $H_2O$ + $H_2O_2$:1:6:1) | 10 min | Boiling |
| HF-dip (2% HF) | 10 s | Room temperature |
| Anisotropic etch | From minutes up to one day | 70–100 |

$$Si(OH)^{++} + 2OH^{-} \rightarrow Si(OH)_4 + Si_{solid}$$ Equation 4.2

The $Si(OH)_4$ formed is easily soluble in KOH thus [23]

$$Si(OH)_4 + KOH \rightarrow H_2O + H_2$$ Equation 4.3

Due to the crystallographic structure of silicon, KOH solution at high concentrations etches {110} planes twice as fast as the {100} planes, and the {111} planes at a rate 200 times slower than the {100} planes [26]. Therefore, when a [100] type silicon wafer, patterned, for example, with straight edge channels is placed in KOH solution with its mask edge aligned in the <110> direction, the exposed surface in the <110> and <100> directions are etched away rapidly until all that is revealed are the slower etching {111} planes, making an angle of 54.7° with the plane of the wafer [23] (Figure 4.2).

Allowing the wafer to be etched further in the KOH solution would eventually lead to a self limiting V-groove structure formed by the abutment of the {111} planes [23] (Figure 4.3). Wet chemical etching also results in significant undercutting of the resist film, thereby affecting the resolution of the patterned opening [28] (Figure 4.4). The average etch rate of a 30% by weight KOH solution at about 70°C is approximately 40μm/hour [26], which implies long exposure of the wafer to the etchant. For trenches in the micron and submicron range, widening of gaps due to surface tension of the solution at the surface of the cleavage may occur [24]. Another limitation of wet chemical etching is that it requires the carrier solution to be continuously agitated while etching cavities since the solution at the surface of the wafer becomes saturated quickly [28].

Since, in this thesis, 4 μm wide 40 μm deep straight walled channels need to be fabricated, the characteristics displayed by KOH wet etching do not seem desirable. Therefore, in order to obtain high resolution straight walled microchannels, characteristics of DRIE were explored.

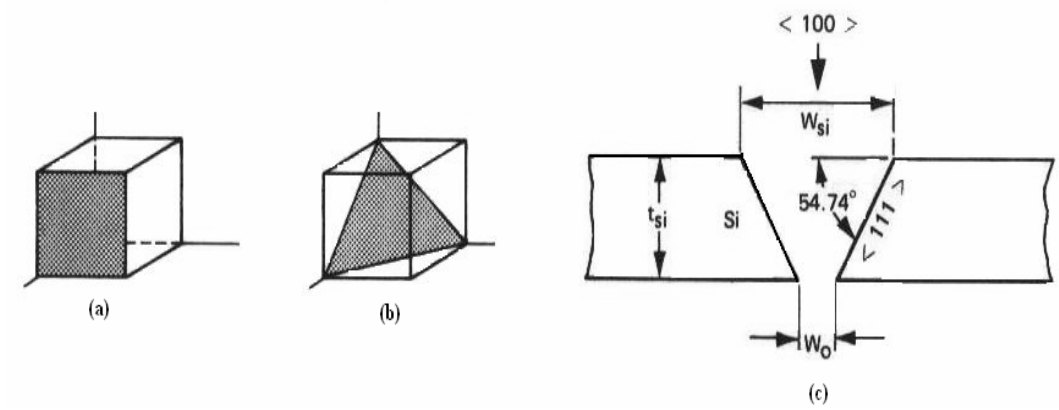


Figure 4.2: Schematic of: (a) (100) plane; (b) (111) plane; (c) anisotropic etching of silicon in (100) plane tending to expose the (111) plane [28]

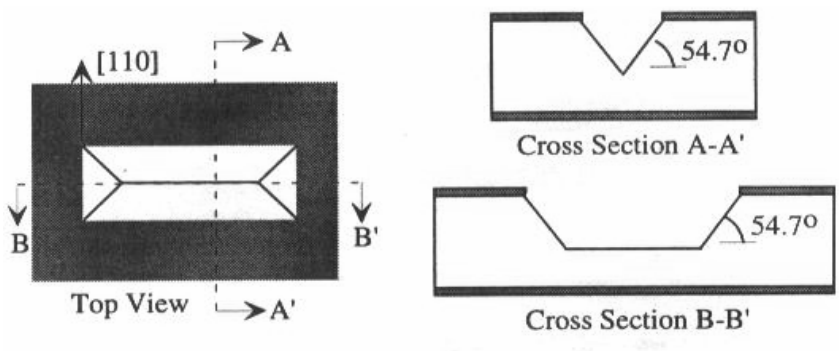


Figure 4.3: Schematic of anisotropic etching of a rectangular opening in a (100) Silicon substrate [23]

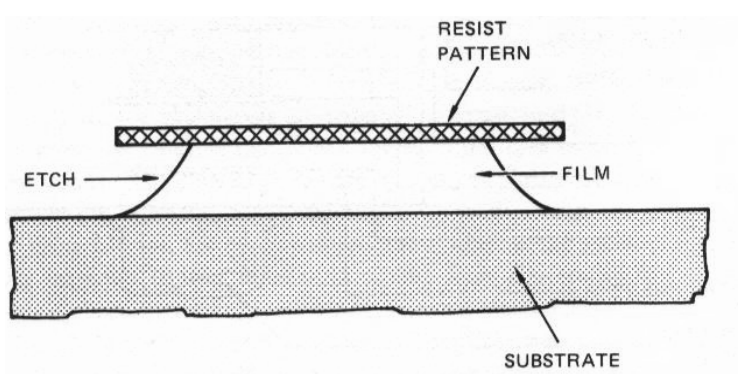


Figure 4.4: Anisotropic characteristic of wet chemical etching causing undercuts in the resist film [28]

## 4.2 DRIE

### *4.2.1 Plasma Generation*

Deep Reactive Ion Etching (DRIE) is achieved by subjecting the surface to be etched to high density plasma of fluorine gases at low pressure [10]. Two common methods of obtaining the plasma for the etching process are Inductively Coupled Plasma (ICP) and Electron Cyclotron Resonance (ECR). In ECR, microwave power at 2.45 GHz is coupled into the ECR to create high density plasma, whereas in ICP, the plasma is generated and maintained inductively at 13.56 MHz [10].

The Alcatel 601E ICP etcher was used to dry etch the required microchannels and the method of fabrication was based on the Standard Bosch Process.

### *4.2.2 Standard Bosch Process*

The Bosch process is a "time multiplexed inductively coupled plasma etch" that uses alternating cycles of etching and passivation to create high aspect ratio trenches of a desired depth in silicon [31] (Figure 4.5). During the etching cycle, sulfur hexafluoride ($SF_6$) molecules, on being excited by the plasma, release fluorine radicals that attack the exposed silicon and form a volatile compound, $SiF_4$ [32] as shown [28]

$$Si_{(solid)} + 4F \rightarrow SiF_{4(gas)} \qquad \text{Equation 4.4}$$

The duration of the etch cycle is about 12 seconds, during which a shallow trench is formed with a nearly isotropic etch profile, which is a characteristic of the fluorine radicals [33]. At the end of this cycle, the $C_4F_8$ source gas is used to deposit a Teflon-like protective film inside the trench [34].

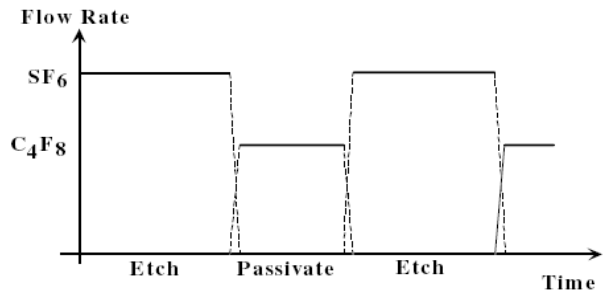


Figure 4.5: Plot of flow rate of gases during alternating cycles of etch and passivation processes over time [33]

$$C_4F_8 \rightarrow C_2F_4 \rightarrow CF_2 \rightarrow CF + F$$ Equation 4.5 [29]

The passivation cycle is shorter than the etch cycle and lasts for about 10 seconds [33]. This step is immediately followed by the etching cycle in which the polymeric layer at the bottom of the trench is removed preferentially in the vertical direction, at a rate much faster than on the sidewall [34]. By the end of this cycle, the polymeric layer on the sidewalls is also removed and the cycle switches to passivation. However, a slight scalloping is observed as a result of the alternating etching and passivation cycles (Figure 4.6).

### *4.2.3 Using Bosch Process to Etch Microchannels*

In order to etch the channels, a (100) p-type Si wafer was spin coated with photoresist AZ 5214, and the pattern of the channels were transferred using the process of image reversal. The wafer was then immersed in a solution of MIF AZ 327 developer for 20 seconds, until the pattern fully developed. This was followed by subjecting the wafer to the Bosch process (Table 4.2) for 6.5 minutes to etch 4 μm wide 40 μm deep trenches.

It was observed that the trenches widened significantly during consequent isotropic etching cycles ($SF_6$) for that entire duration (Figure 4.7).

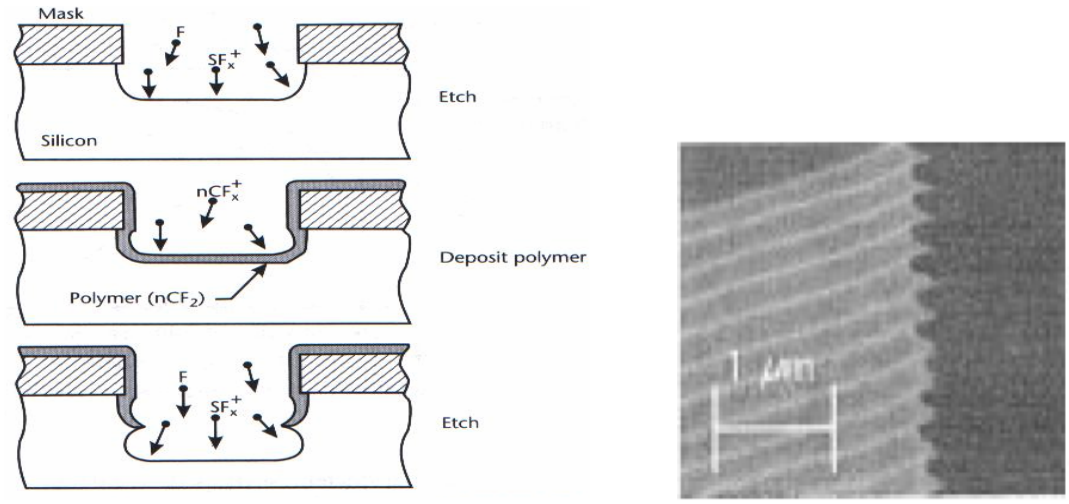


Figure 4.6: [Left] Scalloped sidewalls formed from alternate etching and passivation cycles [27]; [Right] SEM image of high density tip etched in Bosch process showing scalloped sidewalls [31]

**Table 4.2: Standard parameters for the Bosch process in Alcatel 601E ICP**

| Gas Name | Mode | Inactive State Value (sccm) | Active State Value (sccm) | Priority | Active State Duration (s) | Position (%) | Source (W) | Substrate (W) |
|---|---|---|---|---|---|---|---|---|
| $SF_6$ | Pulsed | 0 | 300 | 2 | 7 | 27 | 1800 | 80 |
| $C_4F_8$ | Pulsed | 0 | 130 | 1 | 2 | 27 | 1800 | 80 |

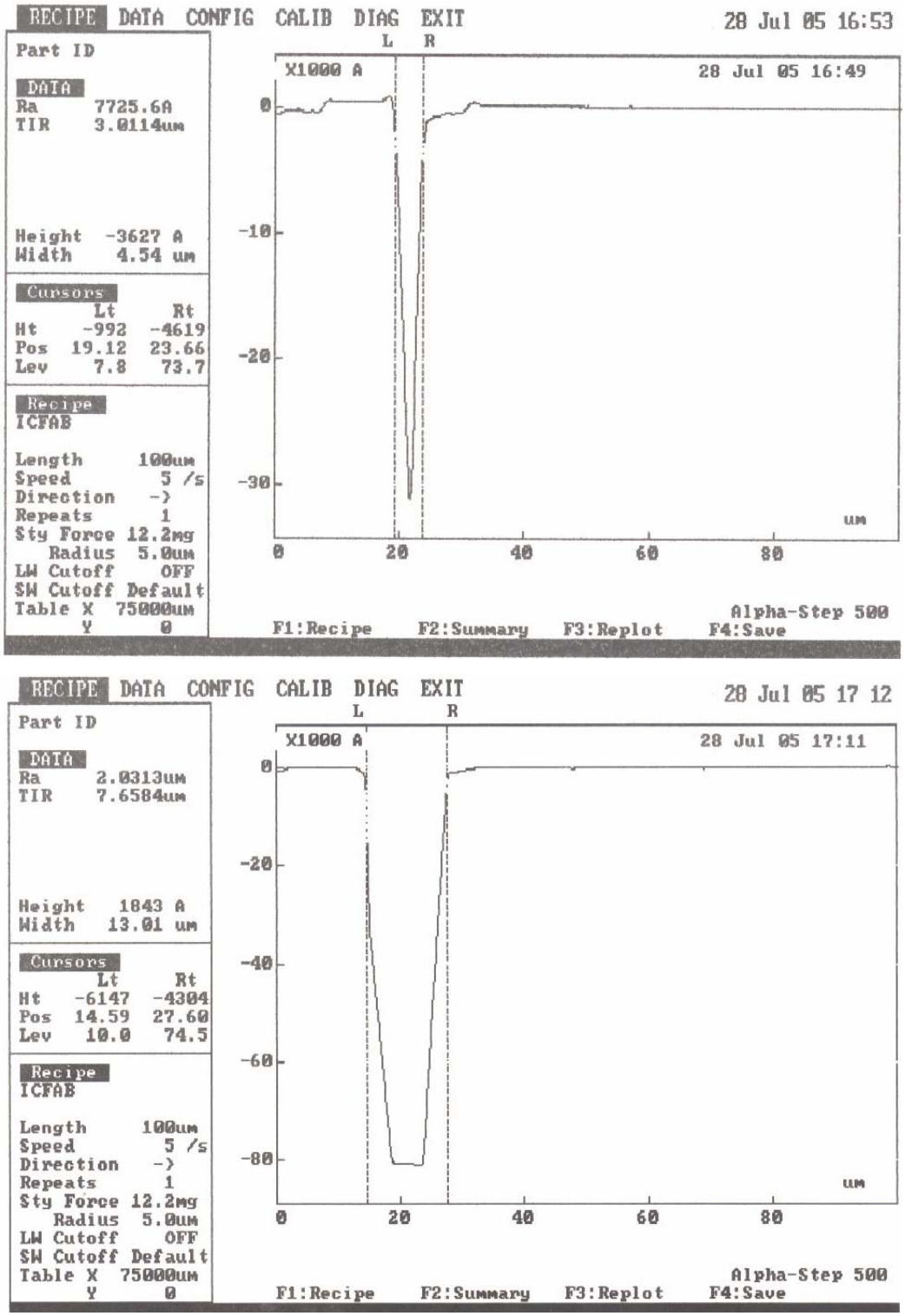


Figure 4.7: Alpha Step 500 Profiler graphs of the width of the microchannel opening; [Top] Before DRIE and [Bottom] after DRIE, using Bosch process; the channel opening shows an increase in width from 4.54 µm to 13.11 µm

Since silicon wafers coated with silicon dioxide have better selectivity of about 150:1 as compared to photoresist coated wafers selectivity values of 50:1 [10], the Bosch process was used to etch the channels coated with silicon dioxide instead of just photoresist. Nevertheless, even in this case the channels continued to widen significantly during the isotropic etch cycles. It was hence assumed that the selectivity of the $SF_6$ gas did not show much variation for silicon dioxide from photoresist for small channels widths of 4 μm. Also, it was desired o have a circular shaped channel up to a depth of 20 μm at the end of the 40 μm trench. This required a dedicated isotropic etch cycle. Therefore, in order to conserve the width of the channel and to scallop a circular opening at the end of the trench, the Bosch process was modified to obtain the desired results.

### *4.2.4 Modified Bosch Process*

The standard Bosch process was revised to include etching and passivation cycles that ran for almost the same amount of time, followed by a constant cycle of $C_4F_8$ deposition for sidewall protection during the final isotropic etching step for the 20 μm circular channel. Table 4.3 summarizes the parameters and duration of the steps used in the altered Bosch process.

The Bosch Rev process is similar to the standard Bosch process on the Alcatel 601E, except that after several trials, the optimum duration of the etch and passivation cycles were modified from 7 and 2, respectively, in the standard Bosch process to 6 and 3, respectively, with all other parameters remaining the same. This process ran for a total duration of 4.5 minutes to etch a 40 μm deep trench of 4 μm width.

In order that the circular channel at the end of the trench may be etched without having to compensate on the width of the channel during the isotropic etching, the Pass process was created to coat the trench with a protective layer. Hence, this process does not use the $SF_6$ cycle.

**Table 4.3: Process steps and corresponding process parameters for the revised Bosch process**

| Process Name | Process Duration (min) | Gas Name | Mode | Inactive State Value (sccm) | Active State Value (sccm) | Priority | Active State Duration (s) | Position (%) | Source (W) | Substrate (W) |
|---|---|---|---|---|---|---|---|---|---|---|
| **Bosch Rev** | 4.5 | $SF_6$ | Pulsed | 0 | 300 | 2 | 6 | 30 | 1800 | 80 |
| | | $C_4F_8$ | Pulsed | 0 | 180 | 1 | 3 | 25 | 1800 | 80 |
| **Pass** | 1.5 | $SF_6$ | Not used | - | - | - | - | 0 | 1800 | 0 |
| | | $C_4F_8$ | Ramp | 0 | 300 | Ramp | 4 | 30 | 1800 | 85 |
| **Student** | 2.33 | $SF_6$ | Ramp | 0 | 300 | Ramp | 3 | 25 | 1800 | 80 |
| | | $C_4F_8$ | Not used | - | - | - | - | 0 | 1800 | 0 |

The $C_4F_8$ passivation cycle is used for duration of 1.5 minutes to deposit the right amount of polymer that would remain for the entire duration of the forthcoming etch cycle. Here, the $C_4F_8$ gas flows in a ramp pattern in increments of 100 sccm for a cycle lasting 4 seconds. After the trench was amply coated with the polymer, the Student process was used to isotropically etch out a 20 μm deep circular channel at the end of the trench. A total of 300 sccm of $SF_6$ gas was used in ramp increments of 100, for cycles of 3 seconds for an entire duration of 2.33 minutes.

Figure 4.8 shows the SEM image of the etched reservoir and channel at a cleaved portion of the wafer, taken on ISI 60A SEM. Measuring the width of the trenches using the Alpha Step 500 Profiler, after the initial Bosch Rev process and the final Student process, very little variation in the width of the channel openings is observed (Figure 4.9). Hence, the modified Bosch process, Bosch Rev and subsequent processes of sidewall protection followed by isotropic etching seemed to conserve the channel width considerably.

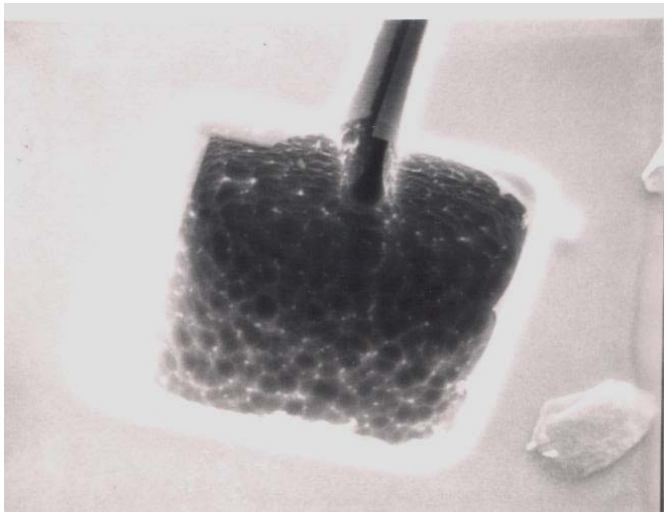

Figure 4.8: SEM image of the needle reservoir with the microchannel inlet at the reservoir end at 300x magnification

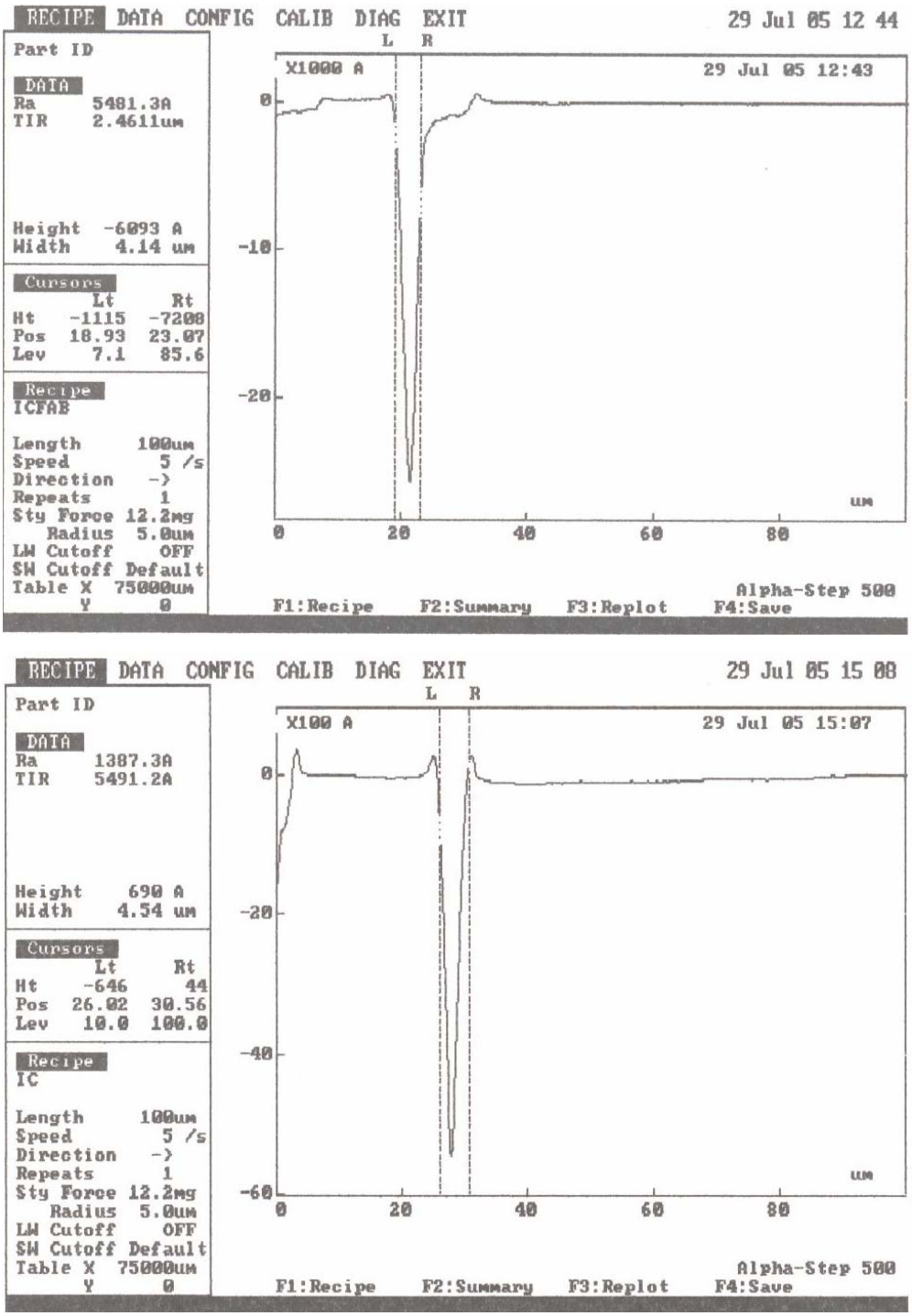


Figure 4.9: Alpha Step 500 Profiler graphs of the width of the microchannel opening etched using revised Bosch process: [Top] After Bosch Rev process; [Bottom] after Student process; the channel opening shows an increase in width from 4.14 µm to 4.54 µm, implying that the channel is width is considerably conserved in the revised Bosch processes

## 4.3 Channel Sealing – PECVD

### *4.3.1 PECVD Oxide*

In a plasma enhanced chemical vapor deposition (PECVD) mechanism, silicon dioxide is deposited on the substrate by reacting separate compounds of silicon and oxygen, such as silane ($SiH_4$) and nitrous oxide ($N_2O$) at low pressure and low temperature of about 300°C [10]. Properties like ease of growth [10] and transparency [35] favored the use of silicon dioxide to seal the channels in this thesis. The Unaxis 790 series PECVD system was used for depositing the required silicon dioxide to seal the microchannels.

In the PECVD process used here, oxide deposition was done using flows of 80 sccm of silane and 900 sccm of nitrous oxide, at a low substrate temperature of 250°C. This yielded a deposition rate of the order of 1 μm/minute of silicon dioxide. The channels were subjected to a number of CVD steps, with regular intervals in between to clean and season the PECVD chamber, during which the sealing status of the channels was experimentally obtained. Figure 4.10 shows the SEM image of an anisotropically etched microchannel sealed with PECVD oxide and cleaved at the center, scanned using a Hitachi S-4500 high resolution SEM. The top view of the sealed channel is shown in Figure 4.11.

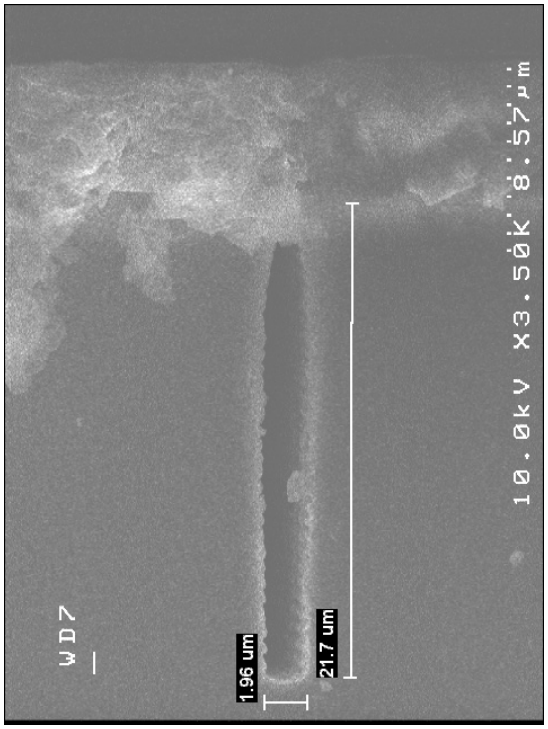


Figure 4.10: SEM image of an anisotropically etched channel sealed with silicon dioxide using PECVD; the scalloped sidewalls, a characteristic of the alternating cycles from the Bosch Rev process is also observed here

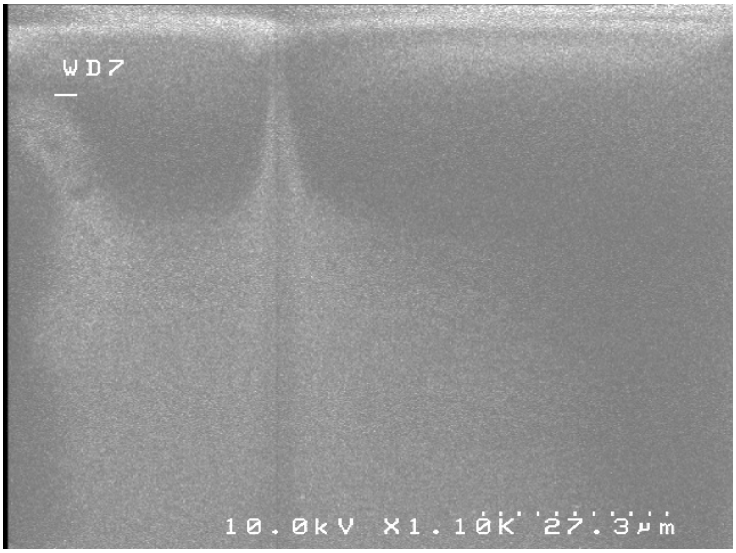


Figure 4.11: SEM image of top view of the sealed microchannel

# CHAPTER 5 MICRONEEDLE BODY FABRICATION

Needle bodies were also fabricated using a p-type <100> silicon wafer. For the needle bodies, different microneedle designs were considered, with emphasis on the needle shape, and placement of the reservoirs and outlet ports. Other important aspects of the needle body that were weighed were length of the needles and the distance between them. Wet as well as dry etching techniques were experimented with. This chapter describes the various approaches taken to arrive at the optimal microneedle design, the suitable masking material, and the appropriate etching technique.

## 5.1 KOH Etching

Initial fabrication processes to obtain the microneedle bodies were primarily based on wet etching of the wafer using 30% by weight of KOH solution. For this, the etching properties of KOH on different mask materials were studied with the purpose of obtaining the most suitable mask material that would withstand long periods of KOH etching, and successfully release the desired microneedles, intact, from the wafer. Metal masks, such as Al and Ti were, however, not tested with as most metals are attacked easily by the alkali metal in the KOH solution, and therefore, such metals do not form a good option as a masking material for prolonged wet chemical etching using KOH.

Also, since through etching of the wafer was required for the release of the microneedles, silicon dioxide could not be used as a mask due to the presence of pinholes in the deposited $SiO_2$ layer, eventually making it susceptible to the etchant [10]. Hence, Cr/Au and silicon nitride, the mask materials most likely to withstand prolonged immersion in the KOH solution, were analyzed. The following sub sections elucidate the different microneedle designs and mask materials that were studied.

### *5.1.1 Chromium/Gold (Cr/Au)*

The very first needle design consisted of a 20,000 x 20,000 µm reservoir and five needles, each 2000 µm in length, housed on an 80,000 x 40,000 µm needle body. Out of the five needles, one had a rectangular tip, whereas the others were tapered at about 15° (Figure 5.1).

For the fabrication of this needle body, positive photoresist, AZ 1813, was spun at 3500 rpm for 30 seconds on to the wafer, and patterned using the Cobilt CA 800 Mask Aligner. After the pattern was developed using the MIF AZ 327, 50 Å of chromium followed by 2000 Å of gold was evaporated onto the wafer using the AIRCO Temescal FC 1800 E-beam Evaporator. The chromium is first deposited on the wafer to enhance adhesion of the gold layer on the polished surface of the wafer.

This step was succeeded by lifting off gold from the undesired areas by submerging the wafer in acetone in an ultrasonic bath. The wafer was then immersed in 30% by weight of KOH solution, maintained at 80°C, and constantly stirred with a magnetic stirrer to maintain the homogeneity of the solution for a uniform etch rate. After approximately 5.5 hours in the KOH solution, the needles were released from the wafer as shown in figure 5.2. However, due to the KOH etching from both sides of the wafer, the thickness of the needles was reduced to 300 µm.

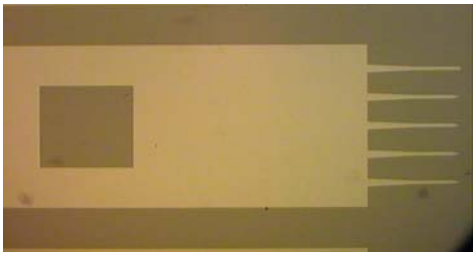

Figure 5.1: Microscope image of a patterned 50Å/2000Å Cr/Au coated wafer, showing the basic design of the needle body with one rectangular needle and four needles tapered at 15°

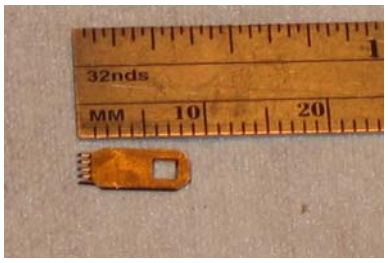


Figure 5.2: Picture of a needle released after 5.5 hours, by the wet chemical etching process using KOH etchant

This, in turn, made the needles brittle, thereby making it difficult to handle the needles without causing some damage (Figure 5.3). It was also observed that due to the property of KOH to selectively etch certain planes faster in comparison with others, all the needles were modified from the original mask as shown in Figure 5.4.

After viewing the results of the first trial, modifications to the needle design were made, increasing the width of the needles and reducing the number of needles from five in the previous design to three in the new design (Figure 5.5).

This design consisted of a 10,000 x 10,000 μm needle body with three different needle shapes; rectangular, isosceles triangular and right triangular needle tips. The total length of the needles was 2000 μm, as was in the first design. But the needles in the new mask were split into a width of 2000 μm and a length of 1000 μm from the base of the needle body, and then into a width of 500 μm for the next 600 μm. The remaining 400 μm formed the height of the needle tips. Each needle also had a 3000 x 3000 μm reservoir with 4 μm wide channels, extending from the reservoir to the tip of the needles.

After patterning the wafer on the polished side, the exact mirror image was patterned, with the help of alignment marks, on the unpolished back side of the wafer, in order to protect the back side of the needle from being etched in the KOH solution, to maintain the thickness of the needle bodies. After evaporation 50 Å/2000 Å of Cr/Au on both sides of the wafer, it was submerged in 30% by weight of KOH solution, as before.

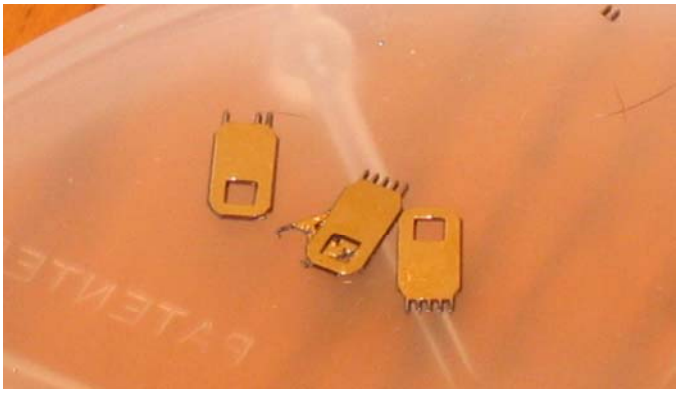

Figure 5.3: Picture of the brittle needle bodies with some of needles broken while handling

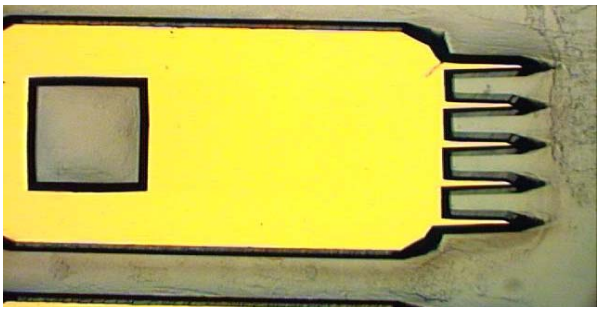

Figure 5.4: Microscope image of needle after three hours of KOH etching showing a modification of the needle tip shapes with respect to the original mask, owing to anisotropic etch characteristics of KOH

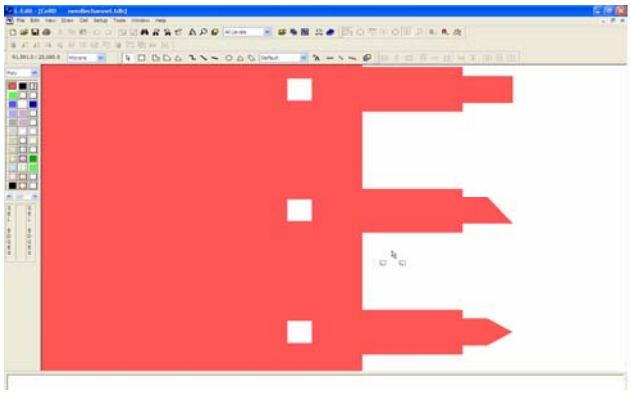

Figure 5.5: Print screen image of the new needle body design created on L-Edit v11.1

After 2 hours of KOH etching, the needles were as shown in Figure 5.6. By the end of the final etching cycle, after 3 hours, most of the microneedles were as shown in Figure 5.7. It was observed that the Cr/Au deposited on the back side of the wafer did little to protect the wafer, as the gold layer did not stick to the unpolished surface for a long time owing to roughness.

As sighted in Reference [36], it is likely that pinholes and cracks could have been formed on the mask material due to high tensile stress, leading to complete etching of the needles. Also, the presence of channels on the needle body, extending from the reservoir to the tip of the needle, combined with the preferential etching characteristics of KOH, yielded badly etched or completely etched needles.

With these observations, it was inferred that masking with Cr/Au did not produce the desired needles, and the next possible choice for mask material, silicon nitride, was tested.

### *5.1.2 PECVD Silicon Nitride*

Silicon nitride is considered a good mask when deep-etching in wet chemical etchants due to its superior chemical properties and higher selectivity compared to silicon [37].

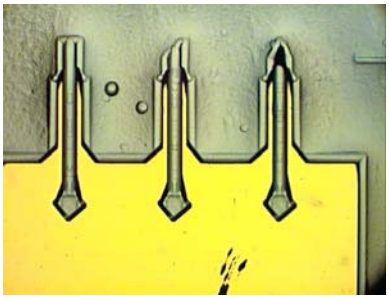

Figure 5.6: Microscope image of needle after two hours of KOH etching showing a change in shape of the reservoir from square to rhombus, and partial etching away of needle due to widening of channel opening

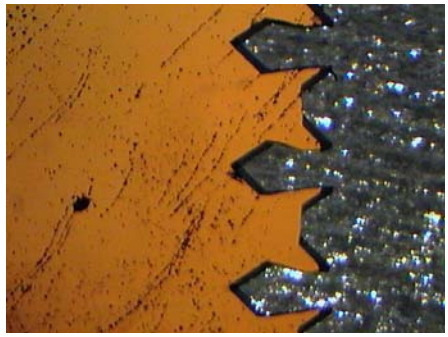

Figure 5.7: Microscope image of the needle body after three hours of KOH etching showing completely etched away needles

With this in mind, 6000 Å of silicon nitride was deposited onto a clean wafer, using Unaxis PECVD system.

In a PECVD process, silicon nitride is deposited at low temperatures of about 350°C, by reacting silane gas with ammonia and nitrogen [38].

$$SiH_4 + NH_3 + N_2 \rightarrow SiN_xH_y + volatile$$

Equation 5.1

After depositing the desired amount of silicon nitride, the wafer was patterned using positive photoresist, AZ 1813, with the very first design described in section 5.1.1 (Figure 5.8). The patterned wafer was then stripped off the photoresist using acetone, and immersed in 30% by weight KOH solution, maintained at 80°C.

After subjecting the wafer to two hours of KOH etching, it was observed that the silicon nitride coating on some of the needles were exhausted even before the needles could be released (Figure 5.9). Most of the needles were also etched away within the first two hours of KOH etching (Figure 5.10). Hence, the process was discontinued as allowing the wafer to be through etched would not yield the desired needles anyway.

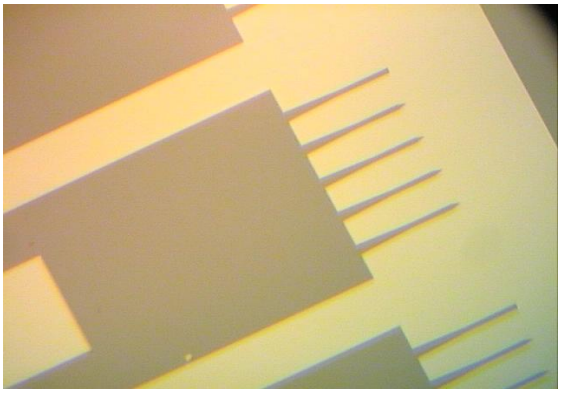

Figure 5.8: Microscope image of image patterned on 6000Å of PECVD silicon nitride

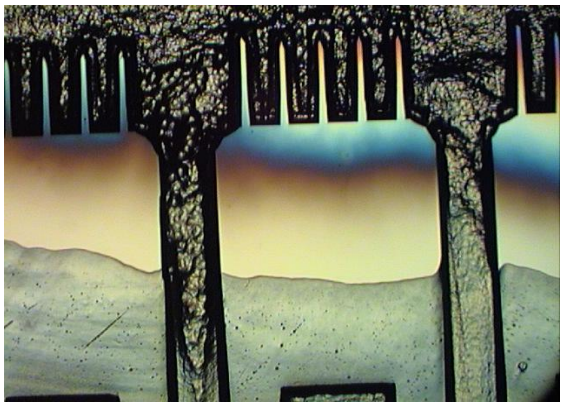

Figure 5.9: Microscope image of needles after two hours of KOH etching showing depletion of silicon nitride well before the needles are released

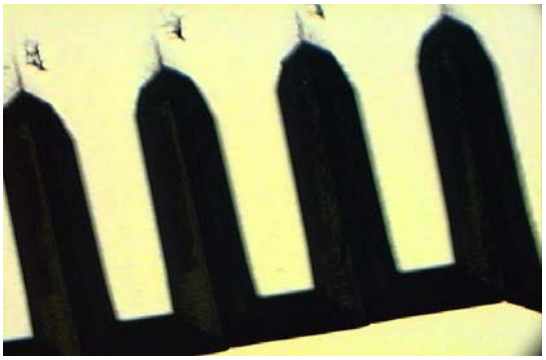

Figure 5.10: Microscope image needles after two hours of KOH etching showing loss of needle shape due to anisotropic etch characteristics of KOH, and needles being etched away well before their release

After researching further into the subject of silicon nitride deposited films, it was noted that a probable reason causing silicon nitride to be exhausted very early during the etching cycle could be attributed to the high hydrogen content in the silicon nitride deposited by the PECVD mechanism [37][10], and also due to the fact that the silicon nitride deposited by this method contains varying amounts of silicon, hydrogen and nitrogen, depending on the process parameters [38], leading to pores in the film.

Based on a tabulated comparison between LPCVD and PECVD silicon nitrides given in Reference [37], silicon nitride deposited using LPCVD mechanism seemed a better option [27]. Moreover, according to Reference [23], in comparison to silicon nitride deposited by PECVD, a thinner layer of silicon nitride would be sufficient to withstand long durations of exposure to the KOH ethchant.

### *5.1.3 LPCVD Silicon Nitride*

In the LPCVD process, deposition of silicon nitride is obtained by the reaction of dichlorosilane and ammonia [39] at a high temperature of about 700°C ~ 900°C, as shown [37];

$$3SiCl_2H_2 + 4NH_3 \rightarrow Si_3N_4 + 6HCl + 6H_2 \qquad \text{Equation 5.2}$$

After depositing 1000Å of silicon nitride using the ASM PECVD DE01 Plasma CVD system, the second mask design described in Section 5.1.1 was patterned onto the wafer and immersed into 30% by weight of KOH solution, maintained at 80°C. The entire etching process took 4.5 hours to release the needles from the base wafer. However, even though the needles bodies that were released were very thick and strong, all the needles were etched away (Figure 5.11). Also, the anisotropic etching properties of KOH widened the reservoir (Figure 5.12). Since very straight etch profiles were desired for the needles bodies, DRIE seemed a better option compared to wet etching using KOH.

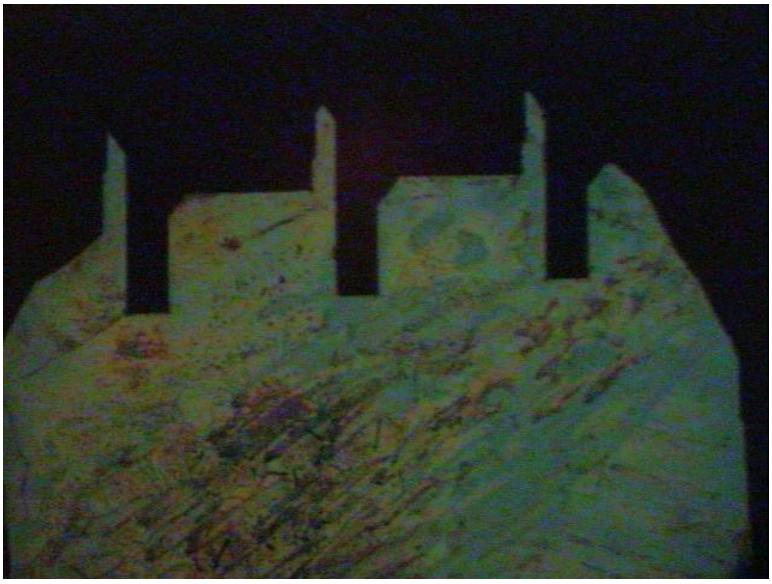

Figure 5.11: Microscope image of released needle after 4.5 hours of KOH etching showing almost completely etched needles, and widening of reservoir and channel

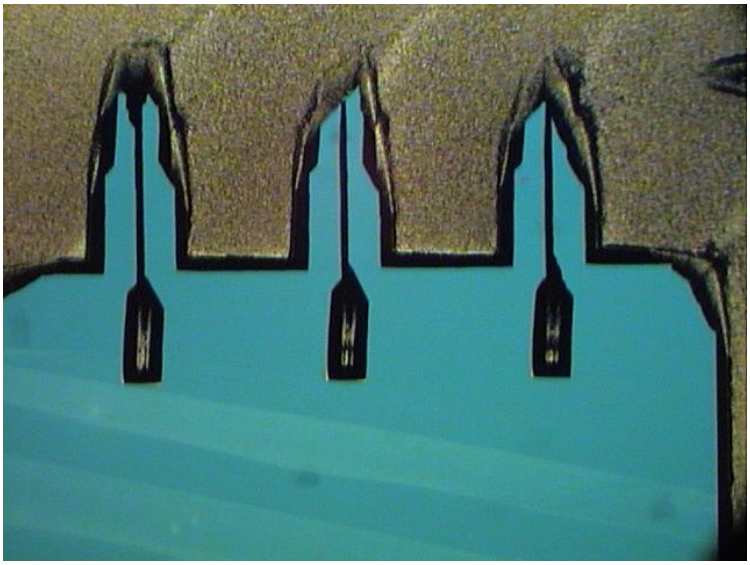

Figure 5.12: Microscope image of released needle after 4.5 hours of KOH etching showing badly etched needles and widened reservoirs

## 5.2 DRIE

Before proceeding to try DRIE for the fabrication of the microneedles, the design of the needles was further modified to enhance delivery of the active compound into the visual cortex of mice. The dimensions of the needle body for the new design, consisting of a needle body 10,000 x 10,000 µm with five needles, arranged in a ramp, and spaced at 100 µm from each other is shown in Figure 5.13 and has been described already in Section 2.1.

### *5.2.1 Photoresist Mask*

After arriving at the appropriate dimensions for the needles, different mask materials were considered for the successful release of the needle bodies with DRIE. According to References [10] and [40], photoresist is one of the best suited mask materials for the standard Bosh process in DRIE. Hence, positive photoresist, AZ 1813, was spin coated at 3500 rpm for 30 seconds, onto the wafer, and the desired pattern was transferred using Cobile CA 800 Mask Aligner.

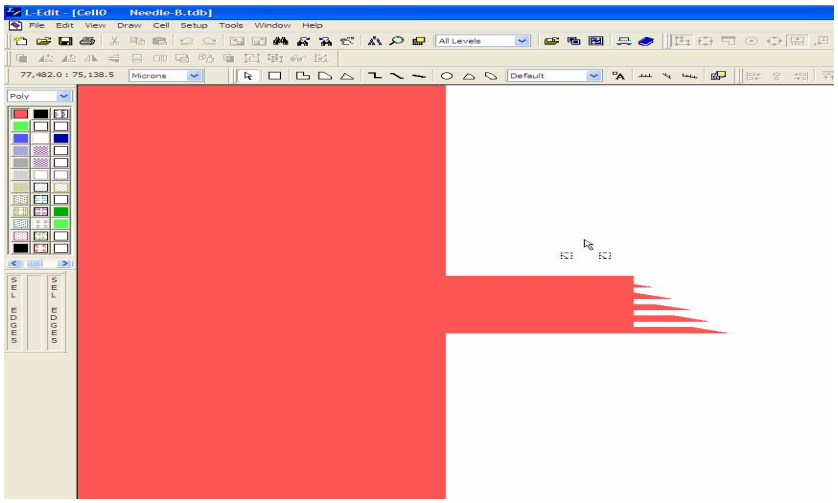


Figure 5.13: Print screen image of the needle design created on L-Edit, version 11.1

After developing the image on the wafer, photoresist from areas to be etched away was lifted off using acetone. The wafer was then set in the Alcatel A601 ICP Etcher, to be through etched using the standard Bosch process. But, at the end of three minutes, even before the needles could be released, the wafer had broken, yielding to stress in the chamber.

### *5.2.2 Aluminum Mask*

Search for a mask material that would withstand longer etch times and enable deeper etching pointed at aluminum [41]. Also, according to Reference [41], a layer of 1000Å thick aluminum is sufficient while etching a 350 μm deep hole in $SF_6/CH_3/O_2$ plasma, due to the non-reactive and non-catalytic characteristic of aluminum to the $SF_6$ and $CH_3$ gases. Use of aluminum for masking silicon in a fluorine plasma supposedly increases the etch rate of silicon, as aluminum remains unaffected by forming more fluorine atoms on dissociating $SF_6$ [40].

So, a clean wafer was coated with 1000Å of aluminum in the AIRCO Temescal FC 1800 E-beam Evaporator, and spin coated with a layer of positive photoresist, AZ 1813, at 3500 rpm for 30 seconds. This was followed by transferring the needle body pattern to the wafer using the Cobilt CA 800 Mask Aligner. After developing the wafer in MIF AZ 327, the back side of the wafer was "glued" to the polished side of another clean wafer using photoresist, to avoid the needles being sucked into the chamber, upon release.

After one hour of DRIE using the standard Bosh parameters, the released needles were as shown in Figures 5.14 and 5.15. Almost all needles, as well as the mask on them, were intact, and closely resembled the original pattern on the mask. Figure 5.16 shows the SEM image of the backside of the needle with the mask on the front, taken on a LEO 1500 series SEM.

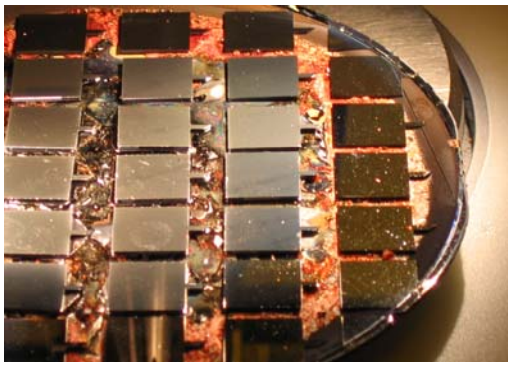

Figure 5.14: Picture of completely etched needle bodies with aluminum mask intact, using DRIE

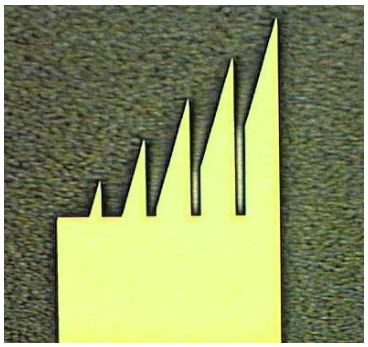

Figure 5.15: Microscope image of the released needle with aluminum mask, after one hour of DRIE

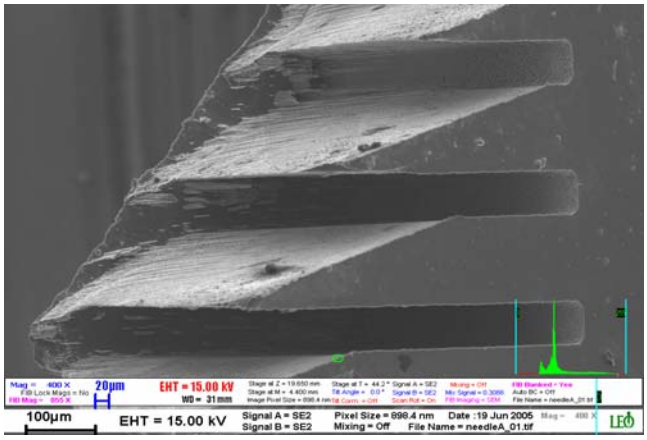


Figure 5.16: SEM image of back-side of released needle with aluminum mask on top, under a magnification of 400 X

# CHAPTER 6 RESULTS AND DISCUSSION

An analysis of the channels and microneedle bodies obtained using the revised and standard Bosch processes, respectively, has been presented in this chapter.

## 6.1 Microchannel

Channels, 6000 μm long, 60 μm deep and 4 μm wide were fabricated using the revised Bosch process (Figure 6.1). The target was to achieve a channel trench of 40 μm in depth, with a circular opening of 20 μm in diameter, at the base of 40 μm trench (Figure 6.2). However, upon viewing the etched channels with a Hitachi SEM, it was observed that the isotropic etch cycle of the revised Bosch process produced an inverted pear-like structure, instead of a perfect circular opening (Figure 6.3), indicating the presence of anisotropic etching during this cycle. A theoretical explanation for this anisotropy, attributing to the "charging phenomenon" is given in Reference [19]. According to Reference [19], anisotropy during the isotropic etch cycle is observed due to a decrease in the etch rate at the bottom of the trench when compared to the lateral etch, owing to a significant difference in the aspect ration of the trench.

Reference [19] also suggests that a more circular trench can be obtained by increasing the aspect ratio of the trench to be etched. This can be done by coating the side walls of the trench with a thicker passivation layer, thereby decreasing the width of the trench [19].

## 6.2 Channel Sealing

The channels were sealed using PECVD silicon dioxide, using Unaxis PECVD. Even though most of the channels were completely sealed, there were some channels that were only partially sealed and some channels that were sealed right to the bottom of the trench

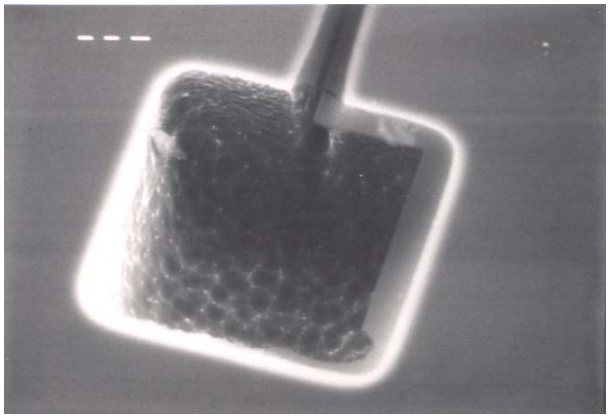

Figure 6.1: SEM image of microchannel at 300 X magnification, fabricated using revised Bosch process

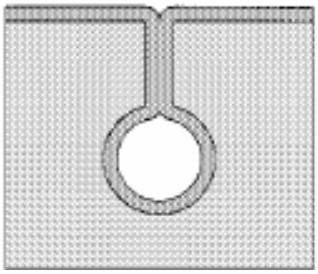

Figure 6.2: Schematic of the desired circular microchannel [19]

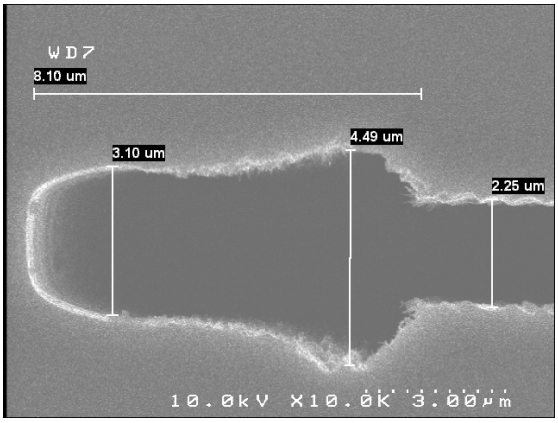


Figure 6.3: SEM image of the microchannel formed during the isotropic etch cycle in the revised Bosch process, at a 10,000 X magnification, showing a pear shaped opening instead of a circular opening, suggesting anisotropy in the etch cycle

(Figure 6.4). This could be due to the variation in particle bombardment at the wafer during deposition in the PECVD system chamber, depending on the placement of the wafer in the chamber, with respect to the grounded and powered electrodes of the PECVD system [10]. Uniformity of deposition could be enhanced by adjusting the temperature of the substrate [10].

## 6.3 Needle Body

The needle bodies were fabricated using DRIE, with aluminum as the mask material. Almost all the needles were released without any damage, and closely matched the original mask. However, although the aluminum mask was intact on all the released needles, images taken on the LEO SEM showed that some of the needles were damaged on the unpolished surface of the wafer (Figure 6.5). It was also observed that the side walls of the needles were not smooth (Figures 6.6 and 6.7), and displayed some amount of undercutting (Figure 6.8).

According to Reference [42], undercutting under the masking layer in the Bosch process increases with etch time due to the isotropic etch step. Hence, the Bosch process could be modified to increase the thickness of the passivation layer to ensure lesser undercut and a smooth profile. Also, etch parameters of the Bosch process could be set to an ascending ramp at each cycle to obtain an even profile with reduced undercut [43].

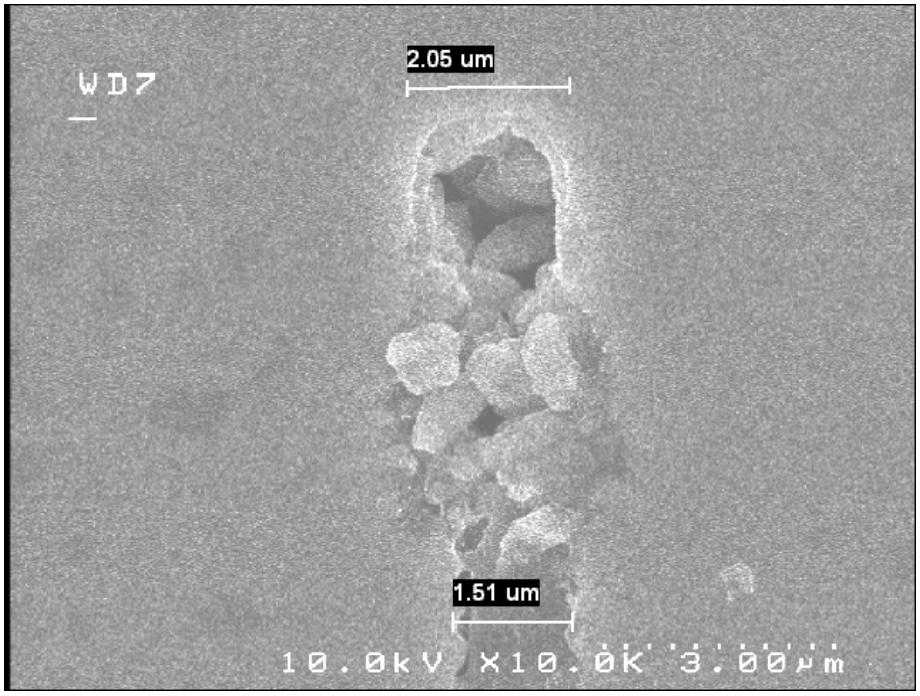


Figure 6.4: SEM image of a channel sealed partially with PECVD silicon dioxide at the bottom of the trench, magnified to 10,000 times the original size

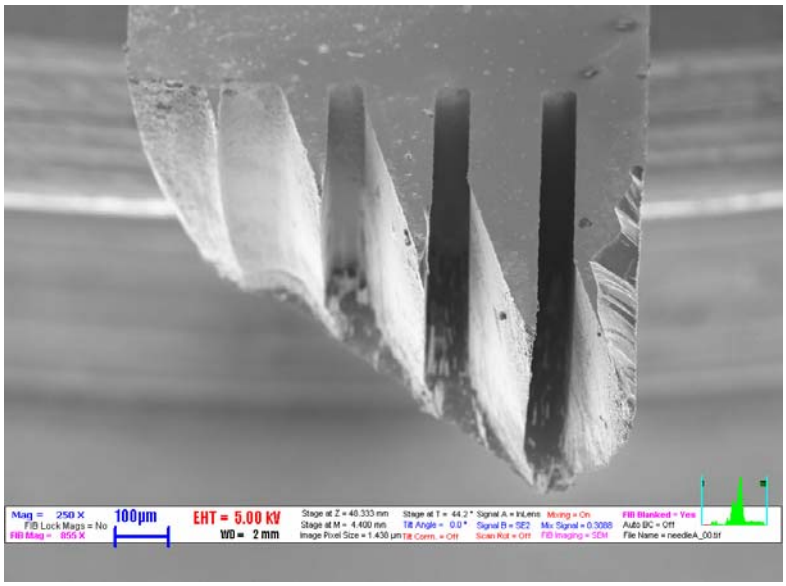


Figure 6.5: SEM image of the back side of a needle released using the revised Bosch process, at 250 x magnification, showing a partially etched needle

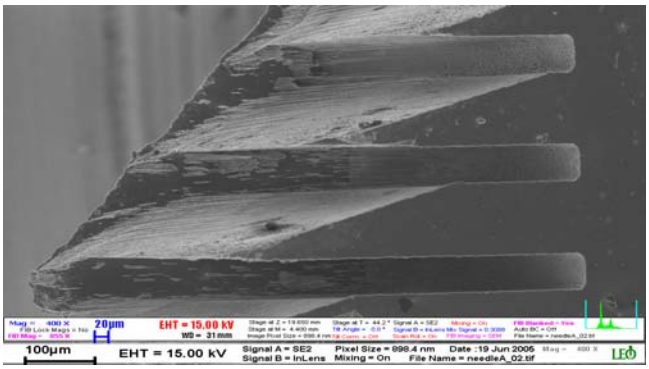


Figure 6.6: SEM image of the unpolished side of the needle released by the revised Bosch process, at a magnification of 400 x, showing rough side walls

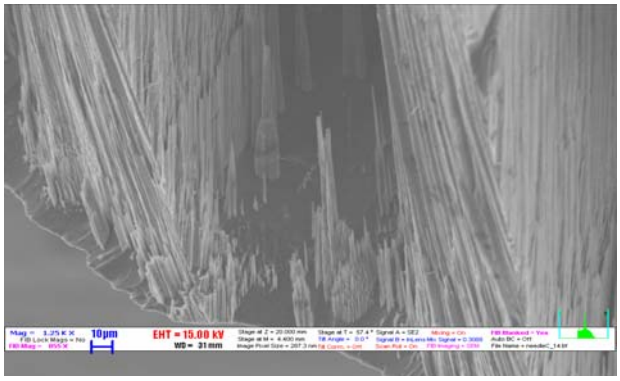


Figure 6.7: Close-up SEM image of the unpolished side of a needle released using the modified Bosch process, at 1250 x magnification, showing rough side walls of the needle

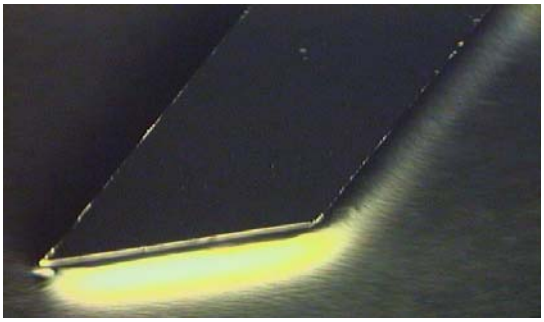

Figure 6.8: Microscope image of a microneedle, after 30 minutes of modified Bosch process, showing undercutting under the mask material

# CHAPTER 7 CONCLUSIONS AND FUTURE WORK

Optimal etching mechanisms for fabricating microneedle bodies and micro channels with silicon have been developed, and the appropriate mask materials that would withstand the long periods of exposure to the etchant required for through etching have been researched.

The etching methods and parameters suggested can further be used to create a silicon microneedle injection system. This can be done by transferring the pattern of the needle bodies and the channels, respectively, on separate wafers, etching and sealing the micro channels, followed by super imposing the patterned needle bodies over their respective sealed channels with the aid of alignment marks, and finally through etching of the entire unit to form individual microneedles.

The fabricated microneedles can then be used to inject the active compound into the visual cortex of mice, in order to study the neural pathways of the nearby ganglion cells. For efficient insertion of the microneedle, the microneedle could be interfaced with a mechanical pump (Figure 7.1), made of a durable material, such as Pyrex. The mechanical pump can be designed using CADKEY (Figures 7.2, 7.3 and 7.4).

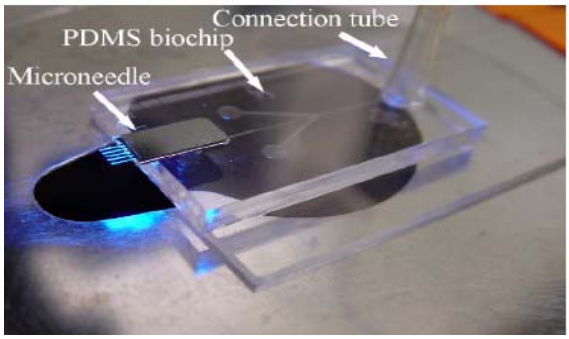


Figure 7.1: Example of microneedle interfaced with a mechanical pump for optimal drug delivery [18]

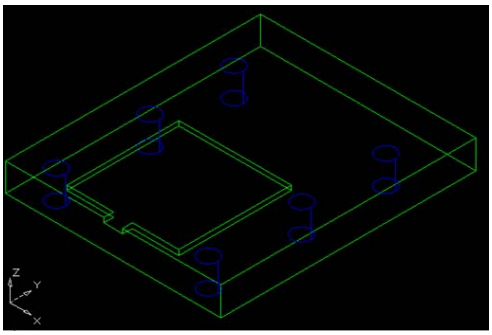

Figure 7.2: Schematic of the base to house the microneedle, designed using CADKEY; the circular patterns indicate position of screws to hold the microneedle in place

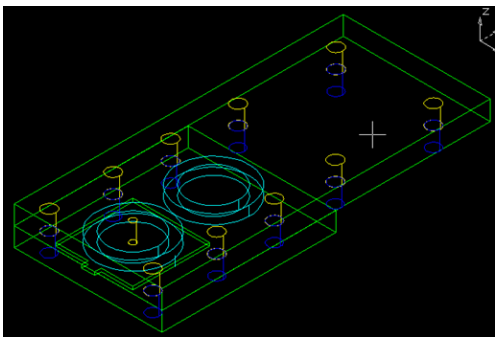

Figure 7.3: CADKEY design of the top part of the mechanical interface unit; the microneedle is held by this with the help of screws, depicted by the smaller circular designs; the larger circles are for providing an inlet for filling the reservoir of the microneedle with the fluid, and for applying pressure to pump the fluid through the microneedle, respectively

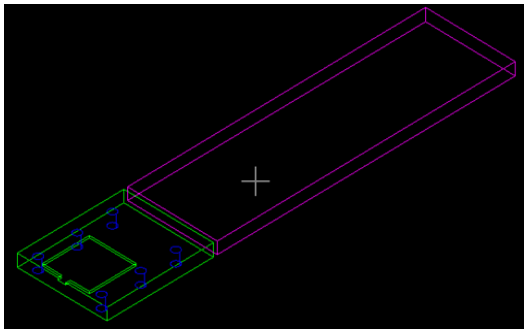

Figure 7.4: CADKEY schematic of the extended handle integrated with the mechanical pump unit to aid robotic control of the microneedle

The needle design suggested in this research could further be modified as shown in Figure 7.5, similar to the works in References [13] and [16], such that a single needle containing several outlet ports can be fabricated for efficient delivery of the fluid drug. Different taper angles for the needle tips can also be experimented with, to minimize area of puncture to the tissue, and to reduce the stress induced to the needle at the point of insertion.

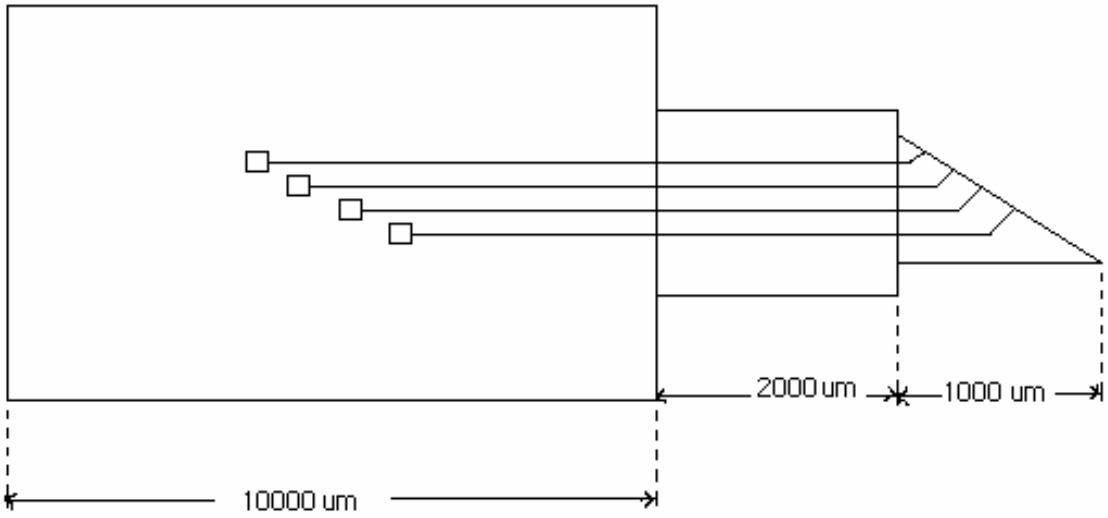


Figure 7.5: Schematic of a microneedle containing multiple outlet ports through a single needle.

# REFERENCES

[1] Devin V. McAllister et al, "Microfabricated Needles for Transdermal Delivery of Macromolecules and Nanoparticles: Fabrication Methods and Transport Studies", Proceedings of the National Academy of Sciences, Vol. 100, Issue 24, pp. 13755-13760, Nov. 25, 2003.

[2] Jung-Hwan Park et al, "Micromachined Biodegradable Microstructures", IEEE International Conference on Micro Electro Mechanical Systems, pp. 371-374, Jan. 19-23, 2003.

[3] Stefan Zimmermann et al, "A Microneedle-Based Glucose Monitor: Fabricated on a Wafer-Level Using In-Device Enzyme Immobilization", IEEE International Conference on Solid State Sensors Actuators and Microsystems, pp. 99-102, Jun. 8-12, 2003.

[4] Devin V. McAllister et al, "Microfabricated Microneedles for Gene and Drug Delivery", Annual Review of Biomedical Engineering, Vol. 2, pp. 289-313, Aug. 2000.

[5] J. D. Zahn et al, "Microfabricated Microdialysis Microneedles for Continuous Medical Monitoring", IEEE-EMBS International Special Topic Conference on Microtechnologies in Medicine and Biology, pp. 375-380, Oct. 12-14, 2000.

[6] Kurt E. Peterson, "Silicon as a Mechanical Material", Proceedings of the IEEE, Vol. 70, Issue 5, pp. 420-457, May. 1982.

[7] S. J. Lee and S. Y. Lee, "Micro Total Analysis System (M-TAS) in Biotechnology", Applied Microbiology and Biotechnology Journal, Springer-Verlag, Vol. 64, pp. 289-299, 2004.

[8] T. A. Desai et al, "Microfabricated Immunoisolating Biocapsules", Proceedings of the SPIE, Vol. 57, Issue 1, pp. 118-120, Jan. 26-27, 1998.

[9] J. D. Zahn et al, "Microfabricated Polysilicon Microneedles For Minimally Invasive Biomedical Devices", Biomedical Microdevices Journal, Kluwer Academic Publishers, Vol. 2, No. 4, pp. 295-303, Dec. 2000.

[10] Marc J. Madou, "Fundamentals Of Microfabrication – The Science Of Miniaturization", CRC Press, Mar. 13, 2002.

[11] Dr. Bruce Gale, “Lecture 10 Wet Etching and Bulk.pdf”, University of Utah, College of Engineering.

[12] W. J. Grande, “Fabrication Technologies for Advanced Heat Transfer Application”, ASME International Conference on Microchannels and Minichannels, Apr. 21-23, 2003.

[13] Jingkuang Chen et al, “A Multichannel Neural Probe for Selective Chemical Delivery at the Cellular Level”, IEEE Transactions on Biomedical Engineering, Vol. 44, Issue 8, Aug. 1997.

[14] Mark R. Prausnitz et al, “Microfabricated Microneedles for Transdermal Drug Delivery”, Proceedings of Bioengineering Conference, Jun. 1999.

[15] Han J. G. E. Gardeniers et al, “Silicon Micromachined Hollow Microneedles for Transdermal Liquid Transport”, IEEE Journal of Microelectromechanical Systems, Vol. 12, Issue 6, Dec. 2003.

[16] Liwei Lin and Albert P. Pisano, “Silicon-Processed Microneedles”, IEEE Journal of Microelectromechanical Systems, Vol. 8, Issue 1, Mar. 1999.

[17] E. R. Parker et al, “Bulk Titanium Microneedles With Embedded Microfluidic Networks for Transdermal Drug Delivery”, IEEE Conference on Microelectromechanical Systems, Jan. 22-26, 2006.

[18] Seung-Joon Paik et al, “In-Plane Single-Crystal-Silicon Microneedles for Minimally Invasive Microfluid Systems”, Physical Journal of Sensors and Actuators A, Vol. 114, Issues 2-3, pp. 276-284, Sep. 2004.

[19] Meint J. de Boer et al, “Micromachining of Buried Micro Channels in Silicon”, IEEE Journal of Microelectromechanical Systems, Vol. 9, Issue 1, Mar 2001.

[20] Jean Berthier, “Microfluidics for Biotechnology”, Artech House, 2006.

[21] Wei-Chih Wang, “Double-Sided Micromachining Process for Silicon Cantilever Using a Parallel Capacitively Coupled Plasma”, SPIE Journal of Microlithography Microfabrication and Microsystems, Vol. 4, Issue 1, Jan. - Mar. 2005.

[22] Benjamin G. Eynon Jr. and Banqui Wu, “Photomask Fabrication Technology”, McGraw Hill, 2005.

[23] Stephen D. Senturia, “Microsystem Design”, Kluwer Academic Publishers, 2001.

[24] L. F. Thompson et al, “Introduction to Microlithography”, Meetings of American Chemical Society on Organic Coatings and Plastics Chemistry, Mar. 20-25, 1983.

[25] Stanford Nanofabrication Facility processes information.

[26] Don L. Kendall and Robert A. Schoultz, “Wet Chemical Etching of Silicon and $SiO_2$ and Ten Challenges for Micromachiners”, Handbook of Microlithography, Micromachining and Microfabrication, Vol. 2, pp. 41-97, 1997.

[27] Nadim Maluf and Kirt Williams, “An Introduction to Microelectromechanical Systems Engineering”, Artech House Publishers, 2004.

[28] Ivor Brodie and Julius J. Muray, “The Physics of Microfabrication”, Springer Publishers, 2001.

[29] W. Graf et al, “Highly Selective Oxide to Nitride Etch Processes on BPSG/Nitride/Oxide Structures in a MERIE Etcher”, IEEE/SEMI Advanced Semiconductor Manufacturing Conference, pp. 314-319, 1998.

[30] H. Seidel et al, “Anisotropic Etching of Crystalline Silicon in Alkaline Solutions – Orientation Dependence and Behavior of Passivation Layers”, Journal of the Electrochemical Society, Vol. 137, No. 11, pp. 3612-3625, Nov. 1990.

[31] Veljko Milanovic et al, “Micromachining Technology for Lateral Field Emission Devices”, IEEE Transactions on Electron Devices, Vol. 48, No. 1, pp. 166-173, Jan. 2001.

[32] Franz Laermer and Andrea Urban, “Milestones in Deep Reactive Ion Etching”, IEEE International Conference on Solid-State Sensors Actuators and Microsystems, pp. 1118-1121, Jun. 5-9, 2005.

[33] A. A. Ayon et al, “Deep Reactive Ion Etching: A Promising Technology for Micro- and Nanosatellites”, Institute of Physics Publishing, Smart Materials and Structures, Vol. 10, pp. 1135-1144, Nov. 2001.

[34] Junji Ohara et al, “A New Deep Reactive Ion Etching Process by Dual Sidewall Protection Layer”, Proceedings of IEEE International on Micro Electro Mechanical Systems, pp. 277-282, Jan. 23-27, 2000.

[35] Choonsup Lee et al, “A Nanochannel Fabrication Technique Using Chemical-Mechanical Polishing (CMP) and Thermal Oxidation”, Proceedings of IEEE International Conference on Nanotechnology, Vol. 2, pp. 553-556, Aug. 12-14, 2003.

[36] Ciprian Iliescu and Francis E. H. Tay, “Wet Etching of Glass”, Proceedings of IEEE International Conference on Semiconductrs, Vol. 1, pp. 35-44, Oct. 3-5, 2005.

[37] Mohamed Gad-el-Hak, “The MEMS Handbook”, CRC Press, Sep. 27, 2001.

[38] S. C. Sorger et al, “Effects of PECVD Hardware Configuration on Mechanical Stress and Stoichiometry of Silicon Nitride Films”, American Institute of Physics International Workshop on Stress-Induced Phenomenon in Metallization, pp. 244-248, 2004.

[39] John Gumpher et al, “LPCVD Silicon Nitride Uniformity Improvement Using Adaptive Real-Time Temperature Control”, IEEE Transactions on Semiconductor Manufacturing, Vol. 16, No. 1, pp. 26-35, Feb. 2003.

[40] M. Elwenspoek and H. Jansen, “Silicon Micromachining”, Cambridge Studies in Semiconductor Physics and Microelectronic Engineering, 1998.

[41] Wei-Chih Wang et al, “Deep Reactive Ion Etching of Silicon Using an Aluminum Etching Mask”, IEEE International Conference on Advanced Semiconductor Devices and Microsystems, pp. 31-34, Oct. 14-16, 2002.

[42] Kitt Wai et al, “Investigation of In situ Trench Etching Process and Bosch Process for Fabricating High-Aspect-Ratio Beams for Microelectromechanical Systems”, American Vacuum Society Journal of Vacuum Science and Technology B, Vol. 20, Issue 5, pp 1878-1883, Sep. - Oct. , 2002.

[43] N. Ranganathan et al, “High Aspect Ratio Through-Wafer Interconnect for Three Dimensional Integrated Circuits”, Proceedings of IEEE Conference on Electronic Components and Technology, pp. 343-348, May. 31 -Jun. 3, 2005.

# VITA

Sangeetha Swaminathan was born in Hyderabad, Andhra Pradesh, India, on 11th October 1982, the daughter of Dr. Thangamma Swaminathan and Dr. S. V. Swaminathan. After completing her work at Padma Seshadri Bala Bhavan Senior Seconday School (PSBB), Chennai, under the Central Board of Secondary Education, she went on to the University of Madras where she studied Electronics and Communications Engineering and received her Bachelor of Engineering in August 2004. With an objective to strengthen her knowledge in Digital Communications, she entered the Graduate School at University of Tennessee at Knoxville in August 2004. Here, she took an interest to Micro-fabrication at the end of the first semester and started working under the able guidance of Dr. Jie Wu from January 2005.